SENSITIVITY OF ELECTRICAL DRIVE PERFORMANCE TO CONTROLLER PARAMETER ERROR

By

Andrew Stephen Babel

A THESIS

Submitted to
Michigan State University
in partial fulfillment of the requirements
for the degree of

Electrical Engineering – Master of Science

2013

ABSTRACT

SENSITIVITY OF ELECTRICAL DRIVE PERFORMANCE TO CONTROLLER PARAMETER ERROR

By

Andrew Stephen Babel

Saturation, cross-saturation, heating of the windings and magnets are nonlinear effects that can affect the measured machine parameters and performance. Because the machine parameters are used in the controller, inaccuracies in parameters will be reflected in the final controller. With parameter error, the controller will not operate as designed. Most studies justify the work of improving controllers and detecting faults by arguing that poor modeling and faults have a deleterious effect upon performance. They fail to completely define the effect on performance. The effect that controller modeling errors have upon performance is described for poor characterization, some minor faults, and the failure to include unmodeled dynamics. The sensitivity of performance to characterization is determined because of the vital nature of accurate parameter determination. Performance effects due to controller parameter error, saturation and other unmodeled dynamics are calculated to justify controller improvements, detailed characterization techniques and fault detection.

ACKNOWLEDGMENTS

I would like to express my deepest gratitude to my advisor, Professor Elias Strangas, whose assistance, advice, and professional guidance have helped greatly in my professional pursuits and development. Without his guidance this thesis would not have been possible.

Additionally, the work performed would not have been possible without the support staff, including, but not limited to: Brian Wright, Gregg Mulder and Roxanne Peacock.

My friends and colleagues have been instrumental in completing my thesis. Their diverse experiences and input have greatly enriched my experience. Their assistance, time, advice, and constant collaboration made this work possible. I would like to thank Jorge G. Cintrón-Rivera and Shanelle Foster for their close collaboration and time, as well as: Reemon Haddad, Cristian Lopez-Martinez, Eduardo Montalvo-Ortiz, Dr. Muhammad Shahid Nazrulla, Feng Niu, Dr. Carlos Nino-Baron, Arslan Qaiser, Dr. Abdul Rahman Tariq, Muhammad Jawad Zaheer, and Dr. Sajjad Zaidi.

My wife Cassandra has given me the crucial love and support I needed throughout this experience. My grandmother Fern Keen has, as always, given me invaluable support, as have my parents, Larry and Janet, and siblings Christina and Matthew.

TABLE OF CONTENTS

LIST OF TABLES

LIST OF FIGURES

KEY TO SYMBOLS AND ABBREVIATIONS

Symbol	Meaning	Units
α	Temperature coefficient of resistance	$\frac{1}{^{\circ}C}$
α_d	Direct axis inductance error coefficient	
α_f	Flux linkage due to the magnets error coefficient	
α_{fd}	Direct axis flux linkage error coefficient	
α_{fq}	Quadrature axis flux linkage error coefficient	
α_q	Quadrature axis inductance error coefficient	
α_r	Resistance error coefficient	
α_s	Nonsalient inductance error coefficient	
χ	Saliency factor of machine	
δ	Current command angle	V
$\Delta_{\xi \to P}$	Sensitivity measure from parameter ξ to performance measure P	V
$e_{abc,s}$	EMF induced in the machine phases	V
$i_{abc,s}$	Stator currents in the stator frame of reference	A
$i^*_{dq0,s}$	Stator current commands in the rotor oriented frame of reference	A
$i_{dq0,s}$	Stator current in the rotor oriented frame of reference	A
I_s	Stator current magnitude	A
i_{sc}	Short circuit current of motor	A
$I_{\mathbf{x}\%}$	Value of **x** percentage of rated machine current	A
K_i	Gain from inverter command to output	
L_{xx}	Self inductance of phase X	H

Symbol	**Meaning**	**Units**
L_{xy}	Mutual inductance given by phases X and Y	H
L_d	Direct axis inductance	H
L_q	Quadrature axis inductance	H
ω_e	Electrical speed of machine	$\frac{rad}{sec}$
ω_s	Operating speed of machine	$\frac{rad}{sec}$
ω_b	Base speed of machine	$\frac{rad}{sec}$
Ω	Mechanical speed of machine	RPM
P	Number of poles in machine	poles
λ_A	Phase A flux of machine	$V \cdot s$
λ_{af}	Flux linkage due to magnets	$V \cdot s$
$\lambda_{dq0,s}$	Rotor oriented flux linkages	$V \cdot s$
R_s	Phase resistance of machine	Ω
R_{s0}	Nominal phase resistance of machine	Ω
T	Torque of machine	$N \cdot m$
T_{abc}	Frame of reference transformation matrix	
θ_r	Electrical rotor position	degrees
T_i	Inverter delay/switching period	sec
T_0	Nominal temperature	$^{\circ}C$
T_s	Current operating temperature	$^{\circ}C$
$v_{abc,s}$	Stator voltage in the stator frame of reference	V
$v_{dq0,s}$	Stator voltage in the rotor oriented frame of reference	V
$v^*_{dq0,s}$	Stator voltage commands in the rotor oriented frame of reference	V

Symbol	Meaning	Units
$V_{l-l,RMS}$	Line to line RMS voltage	V_{RMS}
$V_{\mathbf{x}\%}$	Value of **x** percentage of rated machine voltage	V
$x_{abc,s}$	Generalized stator oriented quantities	
$x_{dq0,s}$	Generalized rotor oriented quantities	
ξ	Machine parameter in question	

Chapter 1

Introduction

It is oft said [9] that electrical machines use greater than forty percent of the world's electricity. This is obvious considering the amount of devices which use them, from washing machines and pumps in the home, traction drives in hybrid and electric vehicles on the road, and serving as electromagnetic actuators in a multitude of industrial applications. With this in mind, any improvement upon the performance of these drives is welcomed. In years past, induction machines served many of these purposes, and would merely be plugged into the wall and allowed to reach steady-state levels and this was sufficient. In modern times the large transient currents, and therefore losses are no longer acceptable. Permanent magnet motors are a fixture of modern drives, as they are more power dense and have smaller losses, as there are no rotor windings. In PM drives, controlling both the flux and torque directly has replaced the blind application of wall voltage and doing this has reduced transient losses. This is accomplished by controlling the current in and out of alignment with the magnet current. Doing this, the machine torque can be precisely controlled at any speed with lesser transient loss than the past.

The use of inverters to apply specific currents to the electrical machine has allowed for the precise control of machine flux and torque, moving past the uncontrolled operation of motors. Two types of controllers exist for the precise control of torque and flux of a permanent magnet machine. The first is a method which directly controls the torque and flux of the machine without controlling the current in [12]. While effective, the goal is maximizing precision, thus current control is used. This rotor oriented method applies currents to control the direct and quadrature axis current and thus the machine torque and flux. The torque is chosen to match that of the load and to allow for the machine to accelerate as desired. The flux is chosen based upon the speed of the machine [5]. This current control method achieves a desired torque at any given speed by the application of specific currents. These models are however dependent upon the machine model inductance, resistance, and the flux linkage due to the magnets. Thus, to have confidence in the performance of the model and therefore control of machine torque at any speed, the individual parameters must be known accurately. Parameter identification can be done analytically, experimentally, or with numerical modeling tools, or experimentally. The goal is to have the parameters be as accurate as possible.

Discussion of the dependence of high performance controllers upon the accuracy of parameters is often not very clear, and involves nonspecific statements. Papers discussing characterization such as [7] cite this as a motivation for their improved characterization method. It is well understood that in order to create a controller some rough parameters must be known, in order to model the machine performance and operation. This begs the question: How will performance be affected if the parameters contain some level of inaccuracy? In closed loop PI control, parametric error will have a limited effect upon the steady-state performance, as the integrator portion of the control will drive the error to zero. In the open loop portions of the control, as in the torque and current relationship, these errors will result in the inaccurate development of torque. Currently, this is avoided by the use of accurate characterization techniques or online parameter estimation as in [8]. To simplify the controller, the former is often chosen over the latter.

In order to improve controllers, the characterization must be as accurate as possible, but if one were to take into account all effects which may be encountered during operation, the characterization process would be much too cumbersome. In order to choose which effects and thus parameters to characterize most accurately, it should be known which parameter is most vital to accurate performance. In order to find this, parametric error is introduced into SPM and IPM machine controllers and the performance changes are noted. Measuring this effect in a standardized way can establish sensitivities for this particular machine and allow the control design to be optimized around those parameters which are most important in the operation of the machine. It is this procedure and simple relationship which is used to optimize characterization procedures and establishes how more accurate characterizations affect the high performance control of these machines. This thesis discusses a method which measures the effect of parametric error upon output performance. This is done analytically, with finite element analysis and experiments.

Chapter 2

Background and Theory

2.1 Machine Modeling

Permanent magnet synchronous machines are valuable for their performance; the magnets used are small, and have a high magnetic flux. Additionally, the fact that the coercivity of the Neodymium Iron Boron and Samarium Cobalt magnets is so high prevents demagnetization at low currents. This allows for the design of small machines with a high of power, thus allowing for small kW-sized machines. A great deal of this size reduction can be attributed to reasons in [6]: the lack of rotor conduction and thus ohmic losses; permanent magnet machines typically have neither field windings nor rotor bars. While the cost of these motors is high due to the magnet cost, the power density compensates.

The machines are typical in their stator design, but the rotor design can vary. In these machines, magnets can either be attached in to the surface of the rotor, or embedded in the rotor as in Fig. 2.1 (a) and (b) respectively. Other machine designs are not investigated and are not included. In the case of the magnets being embedded in the rotor, the inductance is not uniform along the angle of the machine. Machine axes are defined as from the center of the rotor to its outermost edge. There are two main axes: the axis which coincides with the center of the magnet flux and the axis which coincides with the point between the positive and negative fluxes. For reference, note that the positive flux is defined to be the 'north'

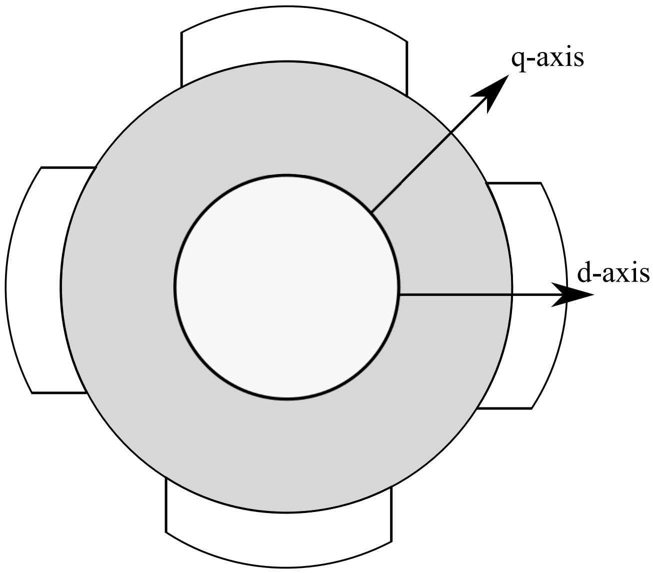

(a) SPM

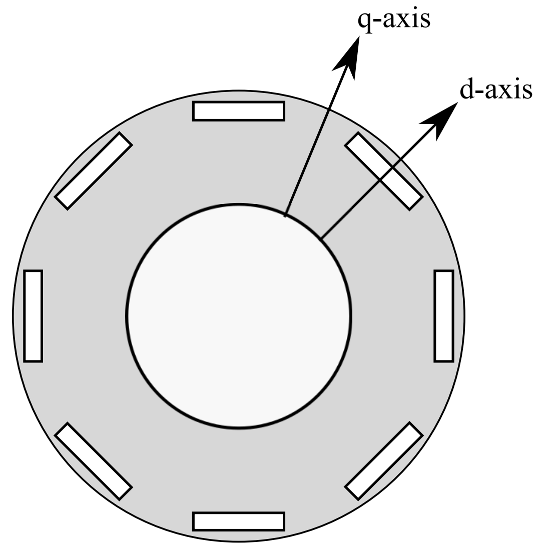

(b) IPM

Figure 2.1: Machine rotor styles

pole or the area in which the flux lines exit the rotor. In the case of the IPM and SPM rotors drawn here, the d-axis coincides with the middle of the magnet. Through the magnet, a flux line along this path would have a large reluctance, since the permeability of the magnet is that of air, which is much smaller than that of the steel which makes up the rest of the rotor.

The machine can be modeled by the phase equations in (2.1). Note that the $e_{\{a,b,c\}s}$ quantities correspond to the emfback-EMF induced in the machine by the magnets. In the IPM machine discussed previously, the difference in permeability of the magnet in comparison with the steel path give rise to the problem of nonuniform inductance. Thus, it makes more sense to develop the equations of the machine in a new two phase frame of reference. This two phase frame of reference is fictitious and is defined to be the axes which align with the magnets and perpendicular to it, so that the inductance in each of these two phases is constant in all cases. This reference frame is defined as the rotor frame of reference.

$$\begin{bmatrix} v_{as} \\ v_{bs} \\ v_{cs} \end{bmatrix} = \begin{bmatrix} R_s & 0 & 0 \\ 0 & R_s & 0 \\ 0 & 0 & R_s \end{bmatrix} \begin{bmatrix} i_{as} \\ i_{bs} \\ i_{cs} \end{bmatrix} + \frac{d}{dt} \begin{bmatrix} L_{aa} & L_{ab} & L_{ac} \\ L_{ba} & L_{bb} & L_{bc} \\ L_{ca} & L_{cb} & L_{cc} \end{bmatrix} \begin{bmatrix} i_{as} \\ i_{bs} \\ i_{cs} \end{bmatrix} + \begin{bmatrix} e_{as} \\ e_{bs} \\ e_{cs} \end{bmatrix} \tag{2.1}$$

The rotor oriented frame of reference for an interior permanent magnet machine is not aligned to the stator, or fixed axes, but the moving, or rotor axes. In particular, it is oriented with the rotor magnet flux axis. The end goal is to have the system be aligned such that the horizontal axis aligns with the middle of the magnet flux. This axis is designated the direct axis. The vertical axis is then set to be ninety degrees ahead of this direct axis, and should be ninety degrees ahead of the maximum positive magnet flux point and ninety degrees behind the maximum negative flux point. Note the axes given in Fig. 2.2, and shown on an example machine in Fig. 2.3. The α and β axes are the horizontal and vertical axes in the stator frame of reference. These do not change position as the machine moves, and are aligned to the machine such that the horizontal axis is in line with the flux developed by the machine with only a positive phase A current. The β axis is merely defined as ninety degrees ahead of this.

Note that the north pole of the magnet is not in alignment with the α axis, due to the rotation of the rotor. The d-axis is always aligned with the rotor pole of the magnet to maintain alignment with the positive flux of the magnet. Thus, if a stator current were applied in alignment with the d-axis, flux would be applied in a direction which strengthens the flux in the machine, while applying a negative d-axis current would weaken the flux. Further, applying a quadrature axis current would induce torque in the machine with a relationship to the rotor oriented axes as in equation (2.2). The value of operating the

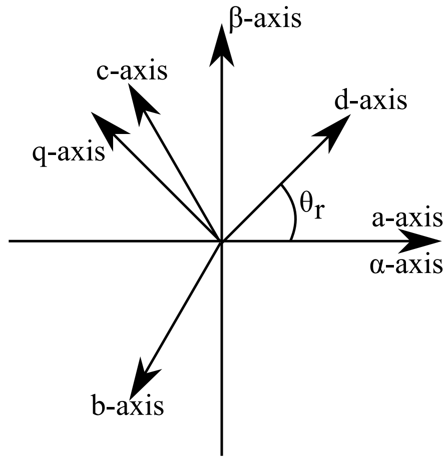

Figure 2.2: Three and two phase machine axes

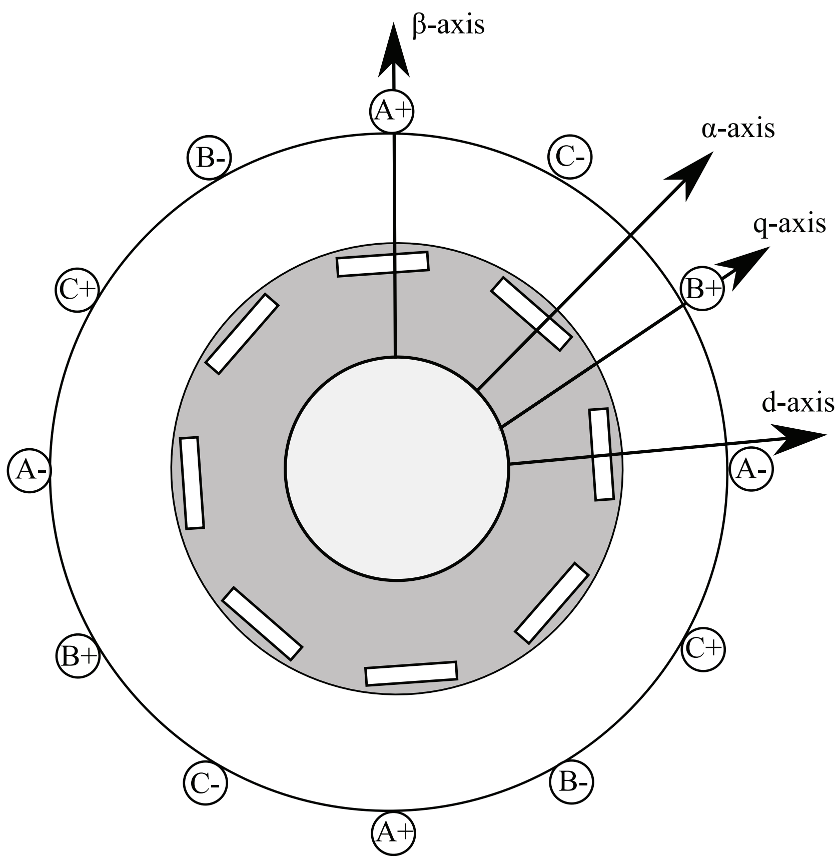

Figure 2.3: Stator and rotor oriented machine axes

machine in this coordinate system can be seen by the simplicity of the torque equation.

$$T = \frac{3}{4}P[\lambda_{af} + (L_d - L_q)i_{ds}]i_{qs} \tag{2.2}$$

The final issue remaining is the application of rotor oriented axis current. This can be done with knowledge of the proper rotor oriented quantities desired, and then applying a transformation (2.4) to achieve the appropriate stator oriented quantities.

$$\begin{bmatrix} x_a \\ x_b \\ x_c \end{bmatrix} = \begin{bmatrix} T_{abc} \end{bmatrix}^{-1} \begin{bmatrix} x_q \\ x_q \\ x_0 \end{bmatrix} \tag{2.3}$$

$$\begin{bmatrix} T_{abc} \end{bmatrix} = \begin{bmatrix} cos(\theta_r) & cos(\theta_r - \frac{2\pi}{3}) & cos(\theta_r + \frac{2\pi}{3}) \\ sin(\theta_r) & sin(\theta_r - \frac{2\pi}{3}) & sin(\theta_r + \frac{2\pi}{3}) \\ 1/2 & 1/2 & 1/2 \end{bmatrix} \tag{2.4}$$

With this understanding, the machine is modeled by equations in this rotor frame of reference as in (2.5)-(2.8).

$$v_d = i_{ds}R_s + \frac{d\lambda_d}{dt} - \omega_e\lambda_q \tag{2.5}$$

$$\ldots = i_{ds}R_s + L_d\frac{di_{ds}}{dt} - \omega_e L_q i_{qs} \tag{2.6}$$

$$v_q = i_{qs}R_s + \frac{d\lambda_q}{dt} + \omega_e\lambda_d \tag{2.7}$$

$$\ldots = i_{qs}R_s + L_q\frac{di_{qs}}{dt} + \omega_e\lambda_{af} + \omega_e L_d i_{ds} \tag{2.8}$$

The machine equations relate the current and voltage with the resistances, inductances and the flux linkage due to the magnets. The resistance R_s is simply the resistance of the phase, L_d is the inductance of the path through the direct axis, L_q is the inductance of the path through the quadrature axis, and the λ_{af} is the flux which links the stator due to the magnets.

2.1.1 Machine Model Considering Saturation and Cross-Saturation

At first glance, the machine model appears to assume that the parameters are constant. In reality, these parameters vary greatly in different circumstances. The resistance is the most obvious, depending upon the temperature of the machine at any given point as well as the frequency applied to the machine due to the skin effect. The flux linkage due to the magnets can change slightly due to saturation of the iron of the machine as well as temperature. The main components that change are the inductances. The L_d can change slightly due to saturation and cross-saturation, but because in both machine cases discussed in section 2.1, the equivalent airgap is large, thus the current required to saturate the machine is much greater than the operating current of the machine. In the case of L_q, because the magnets are embedded, the airgap can become very small. Because of this, when current is applied, much more flux is developed. Because a great deal more flux is developed, the machine will saturate rapidly. This saturation caused by the high level of flux, especially in an IPM machine, is a typical source of variation in the parameters. The typical quadrature axis flux curve shows saturation at large current quantities in Fig. 2.4. Beyond the effect of mere saturation, cross saturation can lead to a reduction in flux in that axis. This is especially true for the quadrature axis with large quadrature axis currents and direct axis currents. This curve in Fig. 2.4 also shows decreasing quadrature axis flux with respect to direct axis current. The saturation changes which affect the machine model can be represented by a

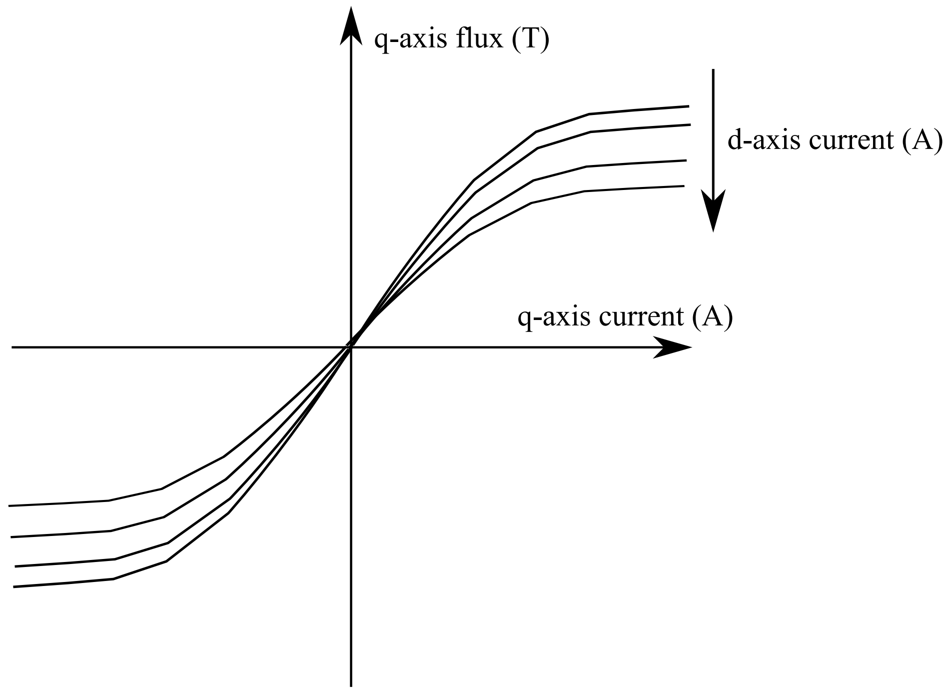

Figure 2.4: B-H curve for a particular material at different current values

machine model which depends on both axis currents as in equations (2.9)-(2.12).

$$v_d = i_{ds}R_s + \frac{d\lambda_d(i_{ds}, i_{qs})}{dt} - \omega_e\lambda_q(i_{ds}, i_{qs}) \tag{2.9}$$

$$\ldots = i_{ds}R_s + L_d(i_{ds}, i_{qs})\frac{di_{ds}}{dt} - \omega_e L_q(i_{ds}, i_{qs})i_{qs} \tag{2.10}$$

$$v_q = i_{qs}R_s + \frac{d\lambda_q(i_{ds}, i_{qs})}{dt} + \omega_e\lambda_d(i_{ds}, i_{qs}) \tag{2.11}$$

$$\ldots = i_{qs}R_s + L_q(i_{ds}, i_{qs})\frac{di_{qs}}{dt} + \omega_e\lambda_{af} + \omega_e L_d(i_{ds}, i_{qs})i_{ds} \tag{2.12}$$

2.1.2 Machine Parameter Determination

In order to design a controller, the machine parameters must be known. These parameters can be determined in a variety of ways, with varying levels of accuracy. The simplest methods are motor standstill techniques, which apply a voltage or current to a machine and measure the rise time to determine the inductance and steady state relation to determine resistance. The flux linkage due to the magnets as well as d- and q- axis flux linkage with applied current must however be calculated by rotating the machine at a constant speed.

The simplest parameter to determine is the resistance as the machine. The measurement does not require the rotor to be moving, and this requires no other parameters. The resistance is measured as in [4] by applying a current to phase A, with the return current coming through the parallel combination of phases B and C. Apply a current for both the rated machine current and 150% the rated machine current. At each current measure the voltage and apply the relationship in equation (2.13).

$$R_a = \left(\frac{2}{3}\right) \frac{V_{150\%} - V_{100\%}}{I_{150\%} - I_{100\%}} \tag{2.13}$$

The flux linkage due to the magnets is also an easy parameter to measure accurately, without requiring any other machine parameters. The back-EMF is the voltage induced by the flux linkage of the magnets. As such, if the machine is open circuited, and the voltage is measured while spinning the machine at constant speed, the flux linkage due to the magnets can be determined. If the line-to-line voltage and speed is precisely applied, the relationship in equation (2.16) is derived from the machine equations with current zero in equations (2.14) and (2.15).

$$v_d = 0 \tag{2.14}$$

$$v_q = \lambda_{af}\omega_e \tag{2.15}$$

$$\lambda_{af} = \frac{V_{l-l,rms}}{\Omega \frac{\pi P \sqrt{3}}{60\sqrt{2}}} \tag{2.16}$$

The resistance and flux linkage due to the magnets are the simplest parameters to calculate due to the simplicity of these tests. The inductance has a similar simple method which is found from a short circuit test on the machine operating at or above the base speed. The machine equations in the short circuit test simplify such that the only current is due to the flux linkage of the magnets, and that this current is in the direct axis. While the machine terminals are shorted and the RMS phase current is measured, the direct axis inductance can be determined as in equation (2.17) if the flux linkage due to the magnets is known, as the induced current is limited by the inductance L_d.

$$L_d = \frac{\lambda_{af}}{i_{sc}\sqrt{2}} \tag{2.17}$$

This direct axis inductance is an excellent measure of inductance if the machine has surface mounted magnets. In this case, the inductances are typically equal in both axes and saturation has little effect due to the large airgap. The assumption of no saturation is insufficient with the IPM machines due to the fact that it measures only the direct axis inductance at one point, at a high current level in the machine. In an IPM motor, this would mean calculating the direct axis inductance, and not having information on either the quadrature axis inductance or the effects of both currents on this quadrature axis inductance value. The aforementioned tests solve this by applying a voltage at standstill and measuring the rise time; the rise time method is the classical inductance determination tool. In order to take into account all current combinations and actual operating conditions, the most sensible characterization method is that of the steady state dynamic characterization. The main method used for inductance calculation has the machine spin at a constant speed while a constant current vector is applied to the machine. With knowledge of the resistance and flux linkage due to the magnets, the voltage is measured and the flux linkages then calculated. This flux linkage depends on both currents and can thus be used for controller development with parameters which will match machine performance during operation like in [7].

Having the machine moving at constant speed with a constant current vector will remove the derivative terms for the currents from equations (2.5)-(2.8), and thus of fluxes in equation (2.18).

$$\begin{aligned} v_d &= i_{ds} R_s - \omega_e \lambda_q \\ v_q &= i_{qs} R_s + \omega_e \lambda_d \end{aligned} \tag{2.18}$$

With the resistance known, the flux depending on both currents can be found from equation (2.19).

$$\begin{aligned} \lambda_q(i_{ds}, i_{qs}) &= \tfrac{v_d - i_{ds} R_s}{-\omega_e} \\ \lambda_d(i_{ds}, i_{qs}) &= \tfrac{v_q - i_{qs} R_s}{\omega_e} \end{aligned} \tag{2.19}$$

Now that accurate machine parameters are known the controller depending on these parameters can be developed.

2.1.3 Machine Control Development

During operation, there are two quantities of importance for proper torque and current development: current commands to generate the torque command and voltage commands to generate the current commands. In order to precisely develop torque, current must be applied to the machine in the correct axes with knowledge of the parameters. This torque relationship was given in equation (2.2). Thus, the desired phase current must be quickly and accurately applied to the machine. All speed current controller systems take the form of Fig. 2.5. In most real world systems, this is done through the use of an inverter applying voltage to the machine terminals and allowing the current to build through use of PI controllers. With perfect machine parameter knowledge, the voltage required for an exact current can be found as in equation (2.20).

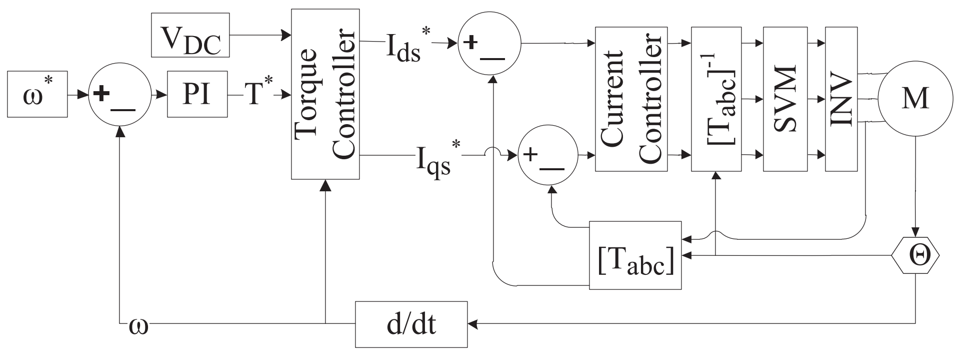

Figure 2.5: Speed controller for machine being characterized with current controller in the inner loop

$$
\begin{aligned}
v_{qs}^* &= R_s i_{qs} + \frac{L_q}{T_i K_i}(i_{qs}^* - K_i i_{qs}) + \omega_r(\lambda_{af} + L_d i_{ds}) \\
v_{ds}^* &= R_s i_{ds} + \frac{L_d}{T_i K_i}(i_{ds}^* - K_i i_{ds}) + \omega_r(L_q i_{qs})
\end{aligned}
\tag{2.20}
$$

On first glance it is clear that there is no integral action in this controller. In fact, with accurate parameters no integral action is needed! In any realized controller, any error in current by application of this voltage would come from errors in the parameters. For this reason, this proportional controller is used to measure the effect of errors in parameters upon the output performance discussed later. This error in performance is the control effort typically applied to the system by this integral action. This is a fairly straightforward method to control the current in either the salient or nonsalient machine case.

2.1.3.1 Torque Control Development

With the machine model the current can be easily applied with the controller previously discussed. While the current controller can be applied to any PM machine, salient or non salient, the torque controller requires more consideration. Initially, only the current commands are needed in order to control torque in an electrical machine. By applying a specific current vector, a specific torque can be expected given the machine parameters and equation (2.2). In the case of a non-salient rotor, the inductances are the same in the torque equation (2.21); the only torque in this case is due to the magnets. Therefore, controlling $\mathrm{i_q}$ can allow for precise torque control. Thus, in this nonsalient case, the torque can be simply controlled by the modified torque equation which includes the fact that the inductances are the same. This equation is solved for the quadrature axis inductance of interest given a torque command in equation (2.23). The trajectory of this current is only along the vertical, quadrature axis as in Fig. 2.6. Quadrature axis current can be applied until the magnitude of this is equal to the maximum current magnitude of the motor.

$$T = \frac{3}{4}P[\lambda_{af} + (L_s - L_s \rightarrow \mathbf{0})i_{ds}]i_{qs} \tag{2.21}$$

$$... = \frac{3}{4}P\lambda_{af}i_{qs} \tag{2.22}$$

$$i_q = \frac{4}{3}\frac{T}{P\lambda_{af}} \tag{2.23}$$

The next main portion of the controller is important when the machine is operating above base speed. In this operating condition, the voltage limit is reached, and thus the operating point is on the circle defined by equation (2.24) and shown by the voltage limit circle in Fig. 2.6, therefore the voltage induced by the magnets must be reduced as base speed is exceeded. To do this, the airgap flux must be reduced. An analytical result is found, that will result in the amount of negative field weakening current to be applied to the machine in equations (2.26) and (2.27).

$$(i_{ds} + i_{sc})^2 + i_{qs}^2 = \left(\frac{\lambda_s^{max}}{L_s}\right)^2 \tag{2.24}$$

$$... = \frac{V_{max}}{\omega_e L_s} \tag{2.25}$$

$$i_{ds} = -i_{sc} + \sqrt{i_{sc}^2(\frac{\omega_s}{\omega_b})^2 + \left[(\frac{\omega_s}{\omega_b})^2 - 1\right](i_{qs})^2} \tag{2.26}$$

$$i_{qs} = \frac{4}{3}\frac{T}{P\lambda_{af}} \tag{2.27}$$

In the case of the controller development, since the inductance is dependent upon the applied current, the currents corresponding to a specific torque and speed command are found computationally. The inductances with respect to he currents must be used. For below the base speed, the relationship between the torque and quadrature axis current is found. Above base speed, for each speed, the resulting torques and voltages are found with the machine model for every current combination. There will be a direct axis current level at which the torque is maximum, and this is the value of direct axis current which will be used for operation at that given speed. Other speeds will exceed the voltage limit while other exceed the current limit. The various limits on the machine are illustrated in Fig. 2.6. Fig. 2.6 shows the current limiting circle, defined merely by the maximum allowable current. The figure also shows the voltage circle, noting that as speed increases, the voltage circle shrinks, as seen by the two different voltage limit circles at ω_1 and ω_2. The circle shrinking can be seen by the speed dependence in equation (2.24). During operation the current applied to the machine must remain within both the current and voltage limit circles. Beyond this,

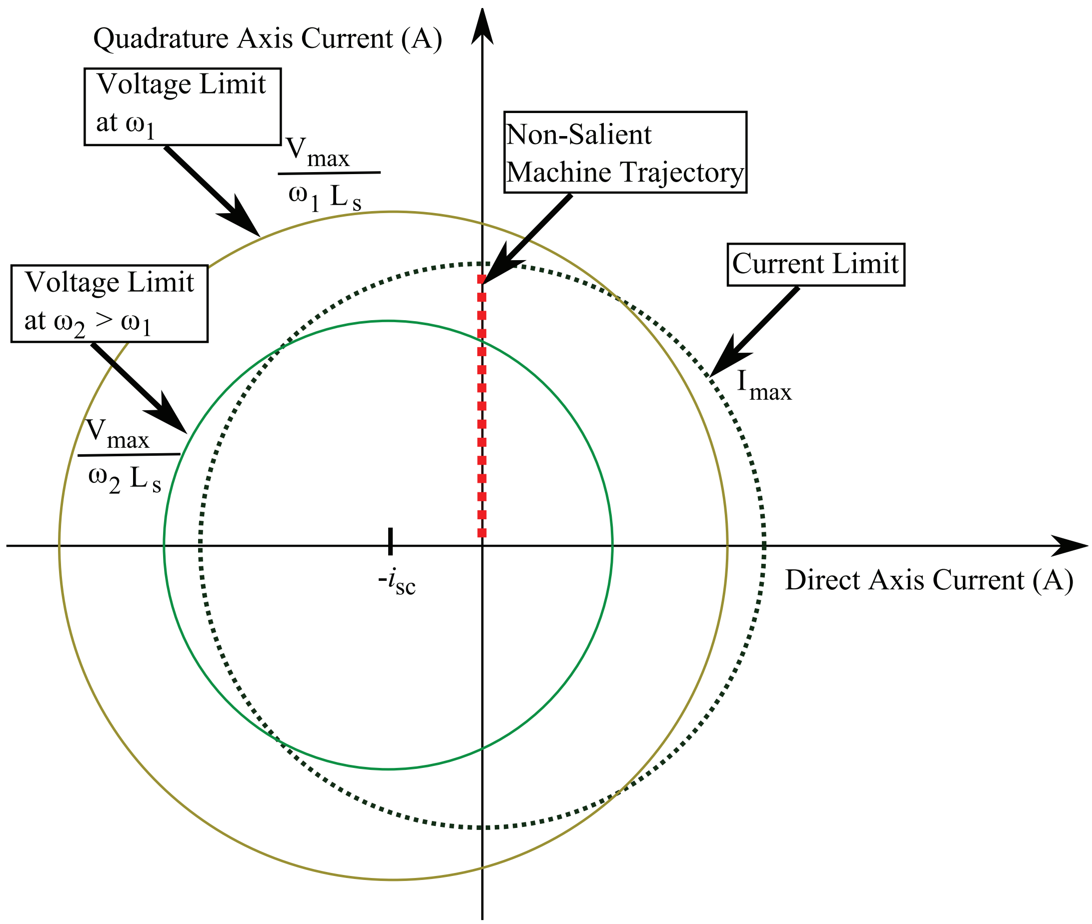

Figure 2.6: Voltage and current limit circles for the nonsalient case. For interpretation of the references to color in this and all other figures, the reader is referred to the electronic version of this thesis.

there exist two cases for machine type. Some machines have the center of the voltage circle, the short circuit current, in the current limit circle. It is this case the thesis discusses since the machine of interest has a short circuit current within the current limit circle.

This trajectory is derived from the ratio of torque to current. For each speed and torque point the minimum stator current is what determines the current and the trajectory. The current requirement that corresponds to a certain Torque/Speed point is added to the controller lookup table as the ideal current condition at that Torque/Speed operating point. This is the point appended to the specified maximum torque per ampere trajectory for each speed. The current trajectories are shown in Fig. 2.7, and can also be found analytically

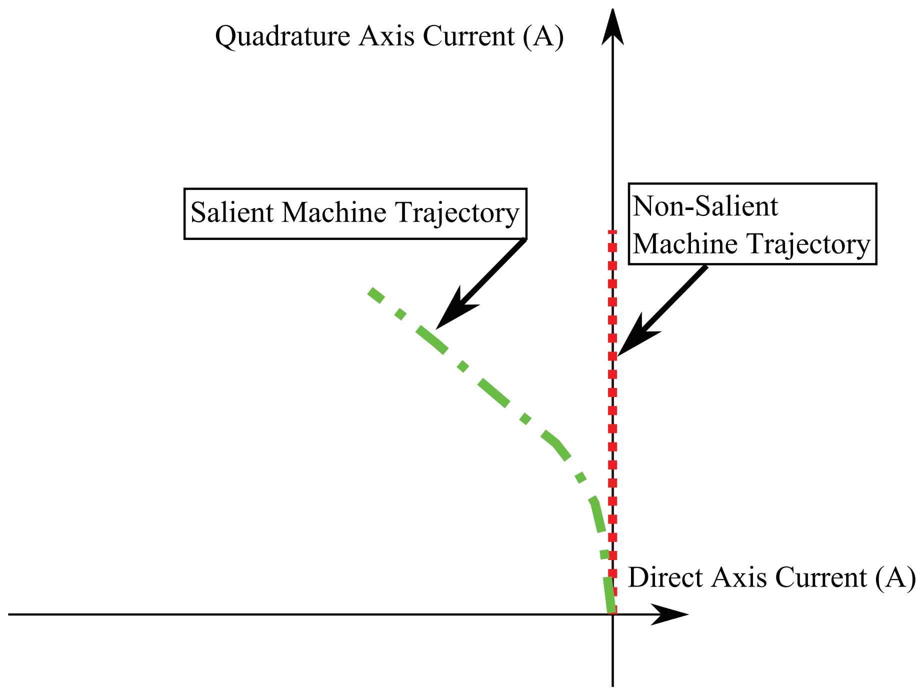

Figure 2.7: Maximum torque per current lines

using the Torque/Current relationship in equation (2.28), which results in (2.32), given some machine information.

If the current limit is reached before the voltage limit, the trajectory must continue along the current limit line as in equation (2.33).

$$\frac{T}{I_s} = \left\{\frac{3}{4}P\left[\lambda_{af} + (L_d - L_q)i_{ds}\right]i_{qs}\right\}/I_s \tag{2.28}$$

$$T = i_q\left(1 - \frac{2\chi}{i_{sc}}i_{ds}\right) \tag{2.29}$$

$$\chi = \frac{L_q - L_d}{2L_d} \tag{2.30}$$

$$i_{sc} = \frac{\lambda_{af}}{L_d} \tag{2.31}$$

$$\begin{aligned} i_{ds} &= \frac{i_{sc}}{8\chi} - \sqrt{\frac{(i_s)^2}{2} + \left(\frac{i_{sc}}{8\chi}\right)^2} \\ i_{qs} &= \sqrt{i_s^2 - i_{ds}^2} \end{aligned} \tag{2.32}$$

$$i_s^2 = i_{ds}^2 + i_{qs}^2 \tag{2.33}$$

A controller designed like this suffices only below the base speed. Above the base speed, the voltage limit is reached, and the machine must be operated at the maximum voltage, or constant flux ellipse. This ellipse (which is for the ideal case of constant inductances) is defined by (2.36) and shown in Fig. 2.8. An increasing speed translates to an ellipse of smaller radius. Using the parameters which are dependent upon the machine current, the voltage and torque for all current and speed combinations are found. Once the commanded torque has been reached, the constant torque line in equation (2.29) is followed by setting the torque constant and finding the least current possible for that torque at a given speed; this defines a line to travel from beyond the base speed until the maximum current line in equation (2.33) is reached. When the constant torque or maintaining a path along the maximum current circle is not possible, the maximum torque per flux line in equations (2.34) and (2.35) is maintained and followed to the horizontal axis as the speed increases.

$$i_{ds} = -i_{sc} + (1+2\chi)\frac{i_{sc}}{8\chi} - \sqrt{\frac{(\frac{V_{max}}{\omega_e L_d})^2}{2} + \left((1+2\chi)\frac{i_{sc}}{8\chi}\right)^2} \tag{2.34}$$

$$i_{qs} = \frac{1}{1+2\chi}\sqrt{(\frac{V_{max}}{\omega_e L_d})^2 - (\kappa + i_{ds})^2} \tag{2.35}$$

$$(i_{ds} + i_{sc})^2 + (i_{qs})^2(2\chi+1)^2 = (\frac{V_{max}}{\omega_e L_d})^2 \tag{2.36}$$

These methods result in motor controllers considering of all parameters. These controllers are used in the operation of the machine.

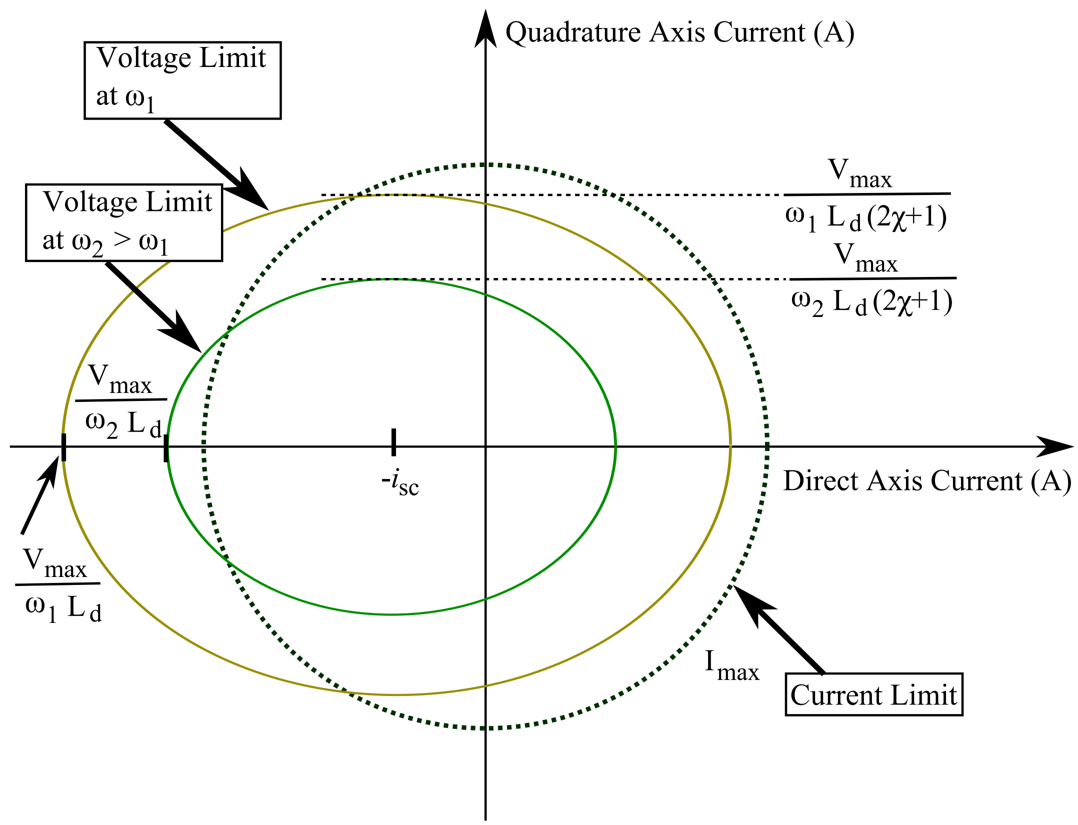

Figure 2.8: Voltage and current limit circles for the salient case

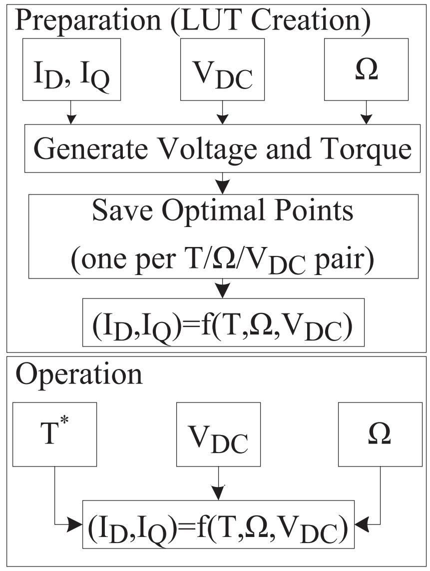

Figure 2.9: Development of lookup table and use during operation

2.1.3.2 Matlab Controller Extraction

In order to design the complete machine controller as it depends upon the current dependent flux linkages a simple analytical method will not suffice in a simple way. This is due to the fact that the flux changes, so the paths will not be as smooth as assumed. Initially, the flux linkages with their dependence upon the machine currents should be found. In addition to these flux linkages, the limits of the machine, including the DC link voltage, phase current limit, phase resistance, number of poles, speed range and current range should be found.

The controller development and utilization are two steps in the process of the development of a working controller, as shown in Fig. 2.9. The first step of preparation begins with: The direct and quadrature axis voltages as well as torque are calculated for each theoretical point. The result of this will be a three dimensional matrix with respect to both currents and speed as in Fig. 2.10.

From this, only the possible combinations are allowed. While the current in either axis

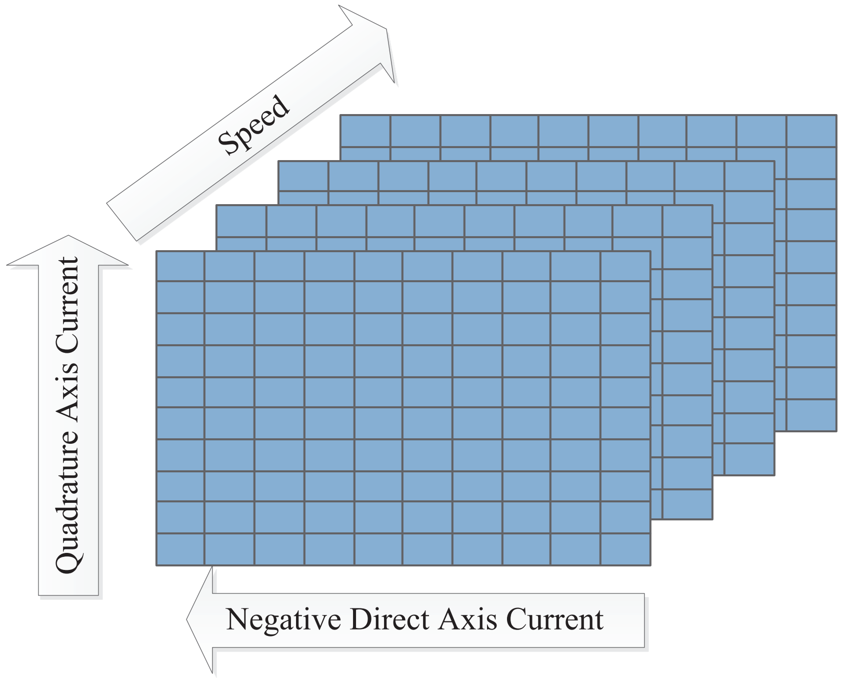

Figure 2.10: Calculation points depending on speed, direct and quadrature axis current

can vary from zero to the maximum allowable current, the magnitude if both axes had the maximum present exceeds the machine limit; the points exceeding these limits are removed. The same applies for voltage, where the voltage points which exceed the level the machine can operate at are removed.

Once this is completed, the optimal operating points will be extracted. In the case of the SPM machine, the direct axis current will be zero for operation below base speed, but constant above base speed. If the direct axis current is too low, the machine voltage limits will be exceeded; if too high, there will be wasted flux weakening, and thus the voltage will be too low. Therefore for both operating regions, finding the maximum torque per unit current will give the optimal voltage point, which will happen to be increasing below base speed and hold to the voltage limit above base speed. Such a line for an SPM machine is

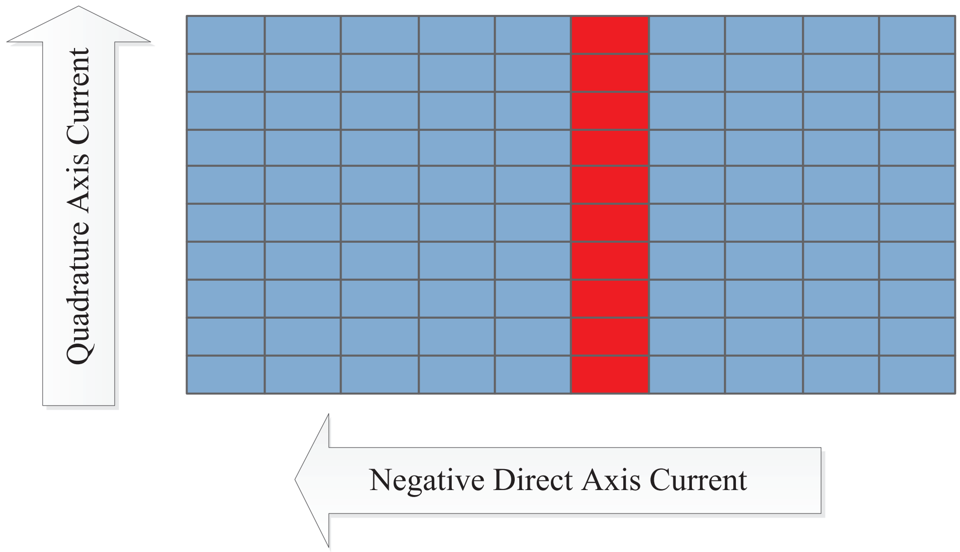

Figure 2.11: Optimal choice of i_{ds} demonstrated for a non-salient machine

given in Fig. 2.11 and is found by incrementing the quadrature axis current and finding for a certain speed and quadrature axis current the direct axis value at which the torque is greatest and current lowest. This method is likewise followed for the IPM machine shown in Fig. 2.12 where even below base speed this calculation results in nonzero direct axis current.

Once this is complete, the only remaining points will be the determination of realizable, optimal points for that current and speed combination. The points can then be assembled into a lookup table. All these points now give us a relationship in equation (2.37), while for torque control we want the inverse relationship. Finding this relationship requires mapping the relationship in the other direction. In order to do this the tables are traversed and for each torque, speed point the least current point, or nearest to the rated voltage is found and added to the set of final operating points. It is this relationship of direct and quadrature

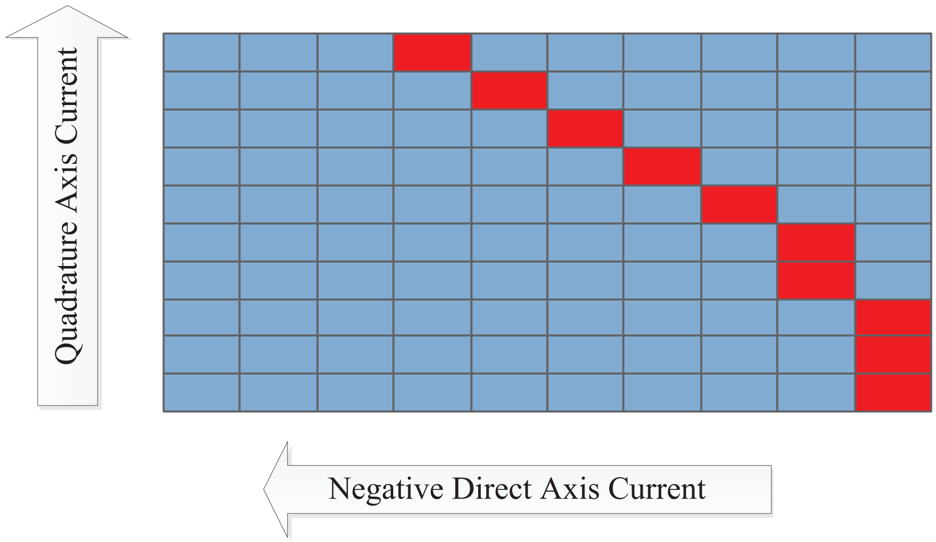

Figure 2.12: Optimal choice of i_{ds} demonstrated for a salient machine

axis currents dependent upon torque and speed which is the lookup table.

$$\begin{bmatrix} I_D \\ I_D \\ \Omega \end{bmatrix} \to \begin{bmatrix} V_D \\ V_Q \\ T \end{bmatrix} \tag{2.37}$$

The only step remaining is the resampling and interpolation of the table to achieve a uniform table with the desired number of points, as is shown in the 'Operation' step in Fig. 2.9. The DSP can then interpolate these values, so an analytical relationship is not needed, and this lookup table will suffice.

2.2 Parametric Error

Parametric error receives the brunt of the blame for controller performance degradation. This is due to the fact the variation in parameters will change the performance of the machine.

In the case of the torque controller for instance, an error in the parameters can result in a different current command than desired. This will then produce a torque either higher or lower than expected. It is the degree of this ‘lower’ or ‘higher’ that is to be quantified with respect to various parameters.

2.2.1 Sources of Parametric Error

2.2.1.1 Characterization Errors

The first and main source of parametric error is the failure to characterize the machine accurately. The main source of this is the assumption that the machine parameters from the manufacturer are true for all machines produced. Typically when a machine is given to the user, the parameters are also given. It is these rough parameters that are mostly used. With a multitude of variations including manufacturing, operating conditions, etc. the parameters can vary from those given by the manufacturer; parameter error is present in situations where each machine is not characterized individually. In addition to the lack of characterization and complete trust in manufacturer parameters, the system used to characterize by the manufacturer may have errors. These errors can be a result of misalignment, sensor, or computational characterization error. The most common characterization error results form the variation in resistance, which is used to calculate the flux linkages; the flux linkages will be incorrect in this case. It is therefore important to do as accurate a characterization as possible to have a controller with achieves precise performance. Having parameters dependent upon as many parameters as possible helps, but typically current dependence will suffice for the salient machine case.

2.2.1.2 Nonlinear Steel Characteristics

A problem source in the case of the salient machine is the fact that the iron saturates. In the non-salient machine, as the airgap is large, the flux developed for a certain current is not very large compared to a machine with a smaller airgap. An IPM machine has a smaller airgap, given that the magnets are embedded in the rotor. Because this airgap is smaller, the flux produced can be quite high. As the level of flux increases, the machine steel saturates. This saturation will reduce the effective inductance of the machine and thus affect the controller greatly. If the control design does not take into account the saturation of the steel, the controller will have a great deal of error. The quadrature axis, having a greater inductance than the direct axis, is most susceptible to this effect. The direct axis is weakly affected by flux, but the current in this axis can cause further saturation in the quadrature axis, especially at higher currents. Thus, the characterization should include a variety of currents in both the direct and quadrature axis to have inductances which depend on these, and thus saturation and cross-saturation. Recall that Fig. 2.4 shows the effect that current can have upon the flux developed and thus the inductance. The inductance depending on this flux is shown in Fig. 2.13.

2.2.1.3 Eccentricity

One case of inductance changing is from a combination of a manufacturing variation and saturation of the machine iron. Eccentricity faults manifest themselves in a rotor being shifted from the concentric position, resulting in the airgap no longer being uniform. This is very possible due to manufacturing as it is very difficult to center the rotor. In the eccentric case, the machine can be divided into two parts, the upper and lower circuit as in Fig. 2.14. The flux developed in the direct axis for instance in this case is greater on the upper circuit

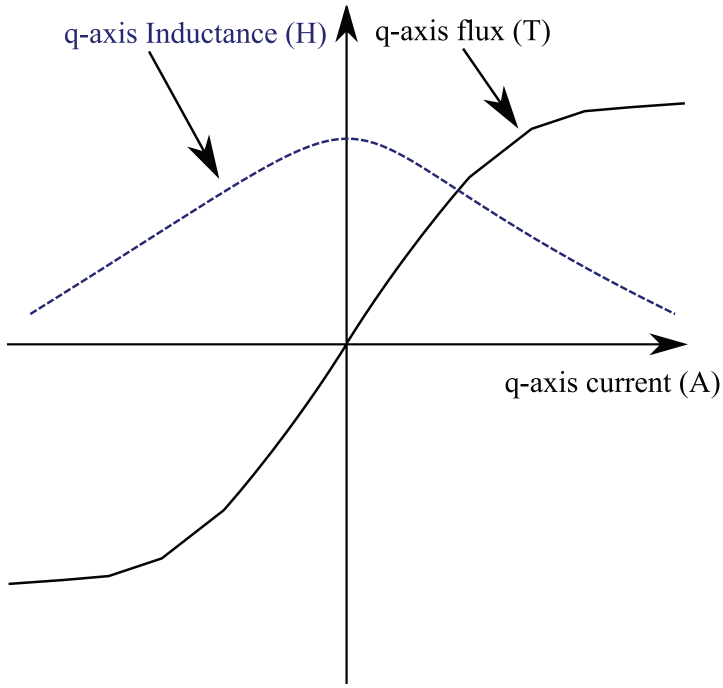

Figure 2.13: Inductance and flux curves showing the effect of saturation in i_q

until the point at which saturation takes effect as in Fig. 2.15, the average of the upper and lower fluxes will be lower than that of the nominal machine. Thus, the flux developed for the same current in an eccentric machine is lower; the lower flux for a certain current corresponds to a lower inductance. From this, it is seen that eccentricity can be a source of parametric error with respect to the inductances. A similar inductance change happens in the quadrature axis inductance. Thus, this is one more reason to accurately know the parameters of the machine and the effects of parametric error.

2.2.1.4 Uniform Demagnetization

Uniform demagnetization is a phenomenon where the magnets of the machine all lose the same amount of remnant flux. This is a problem for torque development, which is heavily dependent upon the flux linkage due to the magnets. This phenomenon is not uncommon, as the rare-earth based magnets can become demagnetized at high, but possible temperatures.

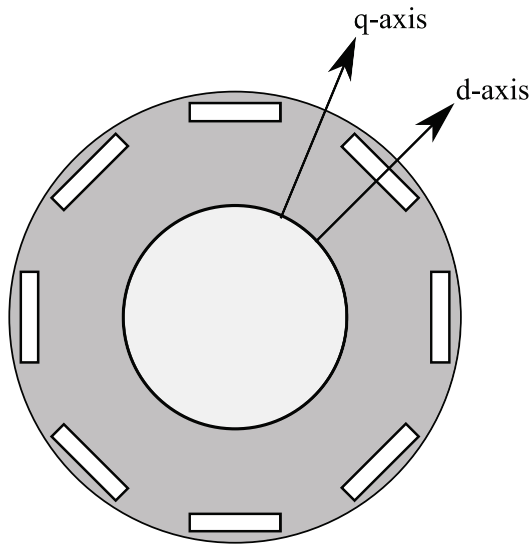

Figure 2.14: Eccentric IPM machine model

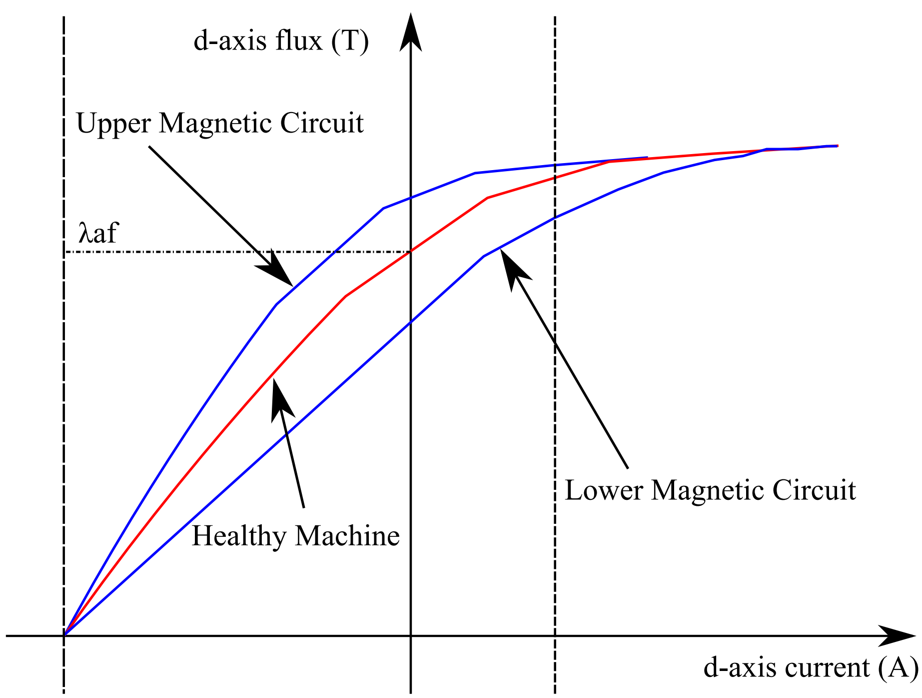

Figure 2.15: Flux curve for an eccentric and concentric machine (Based on a graphic in [3])

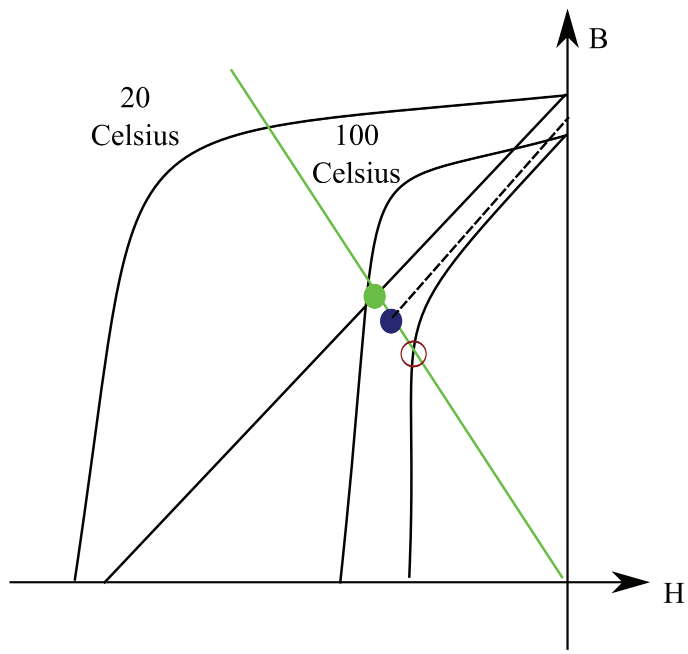

Figure 2.16: Flux curve for demagnetized machine (Based on a graphic in [11])

This is due to the fact that the magnetic hysteresis curve is shifted during high temperatures, because the coercivity is reduced.

Note the plots of flux on the flux density and field intensity axes in Fig. 2.16 with the intrinsic and normal curves of the flux for both 20 $^{\circ}C$ and 100 $^{\circ}C$. If at 20 $^{\circ}C$ the operating point on the normal curve is the light green dot. If the magnet temperature rises to 100 $^{\circ}C$ the new operating point is given by the hollow circle with a red outline. Because this operating point is below the knee of this curve, operating point does not return to the original operating point, but a new operating point. This new operating point is given by the dark blue dot, and the remnant flux of the magnet reduced to the intersection of the dashed line with the flux density axis. This is therefore important, as the remnant flux density is reduced, which will affect control performance; for this reason we seek to quantify the effect of demagnetization upon controller performance.

2.2.1.5 Heating

It is well known that as the windings of a motor are heated, the resistance of these windings change. This is a common occurrence during prolonged operation, as is common in these machines. The resistance changes with the relationship given in equation (2.13) from [10]. This simple relation is the motivation for studying resistance errors in the control of machines.

$$R_s = R_{s0} + \alpha R_{s0}(T_s - T_0) \tag{2.38}$$

This relationship is found from R_{s0}, the resistance at an initial temperature T_0,. Further, α is the temperature coefficient for the material which is copper ($2.92\text{E} - 3\frac{-}{^\circ\mathrm{C}}$) and T_s is the temperature of concern.

2.2.2 Effect of Parametric Error Upon Performance

An analytical method is used to predict the variation of performance with respect to changing parameters from [5]. This method is expanded upon to include all parameters and include operational analysis at all speeds. The analysis performed will concern five sets of equations: the current controller equations (2.39)-(2.42), the nonsalient torque equations (2.43)-(2.44), the salient torque equations (2.45)-(2.46), the flux dependent torque equation in equations (2.47)-(2.48), the nonsalient voltage circle equations (2.49)-(2.50), and the salient voltage ellipse equation (2.51)-(2.52). Note in these, the quantities with errors present are denoted by their primed values. α is a fraction used to show variation in a parameter. The X' is the value of incorrect X parameter assumed. α_d, α_q, α_r, α_s, α_f, α_{fd}, and α_{fq} represent the d-inductance, q-inductance, resistance, stator inductance in the nonsalient case, flux linkage due to the magnets, direct axis flux, and quadrature axis flux fraction errors. These

Table 2.1: Operating point quantities

Parameter	Description	Value
ω_e	Electrical Motor Speed	$167.6\left(\frac{rad}{sec}\right)$
L_d	Direct Axis Industance	$48.7(mH)$
L_q	Quadrature Axis Inductance	$86(mH)$
λ_d	Direct Axis Flux Linkage	$0.55(V \cdot s)$
λ_q	Quadrature Axis Flux Linkage	$1.021(V \cdot s)$
I_d	Direct Axis Current	$-6.604(A)$
I_q	Quadrature Axis Current	$11.87(A)$
T_i	Inverter switching period	$100(\mu sec)$
R_s	Phase Resistance	$1.4(\Omega)$
λ_{af}	Flux Linkage due to the Magnets	$0.87(V \cdot s)$

values are allowed to range anywhere from 0 to 2, where 1 represents accurate parametric knowledge. For this analysis, the third machine used in this paper with an actual operating point and experimental data. The parameters from this are given in Table (2.1).

In the case of the current controllers, with multiple parameters, a graphical approach is taken to analyze the parametric sensitivity. The equations in (2.39)-(2.42) show the voltage command equations with respect to their actual parameters, commands and α error fraction. In order to do this analysis, these equations are solved for their actual current value. Assuming that the controller parameters remain constant, and the machine parameters change, the changing voltage command with respect to parameters can be found. This is of interest because the machine parameter change could cause voltages to be applied which are out of the machine voltage operating range. Even when within the limits, voltage command errors will translate to errors in the developed current. In Fig. 2.17, it can be seen that the direct axis inductance has a significant effect, while quadrature only has a significant effect at low values of quadrature axis inductance. Fig. 2.18 shows that resistance has little effect on the direct axis voltage command, and that the flux linkage due to the magnets clearly has no effect because the equation does not depend upon the flux linkage to to the magnets. Fig. 2.19 shows that the direct axis inductance does not have a large effect, which the quadrature axis inductance does. Finally, Fig. 2.20 shows the flux linkage due to the magnets has a significant effect while resistance less so. Note that the flux linkage due to the magnets has a lesser effect than normal as the machine is heavily loaded, and as such the voltage is mostly determined by the resistance and inductance.

$$v_{qs}^{*\prime} = R_s' i_{qs} + \frac{L_q'}{T_i K_i}(i_{qs}^* - K_i i_{qs}) + \omega_r(\lambda_{af}' + L_d' i_{ds}) \tag{2.39}$$

$$... = \alpha_r R_s i_{qs} + \frac{\alpha_q L_q}{T_i K_i}(i_{qs}^* - K_i i_{qs}) + \omega_r(\alpha_f \lambda_{af} + \alpha_d L_d i_{ds}) \tag{2.40}$$

$$v_{ds}^{*\prime} = R_s' i_{ds} + \frac{L_d'}{T_i K_i}(i_{ds}^* - K_i i_{ds}) + \omega_r(L_q' i_{qs}) \tag{2.41}$$

$$... = \alpha_r R_s i_{ds} + \frac{\alpha_d L_d}{T_i K_i}(i_{ds}^* - K_i i_{ds}) + \omega_r(\alpha_q L_q i_{qs}) \tag{2.42}$$

In the nonsalient torque equation as given with the parameter scaling factor in equation (2.44), the effect of the changing flux linkage quantity can be investigated. As α_f is reduced below 1, or as the flux linkage due to the magnets is reduced, the torque expected is reduced. Thus, for the maintenance of the desired torque, more current would need to be applied. This in effect lowers the torque limit, as the machine rated current remains constant. Similarly, if this α_f is increased to 2, the torque expected is doubled for the same current. The actual torque developed in an open loop torque controller will be half, as we apply only half of the current of interest to get the previously desired torque. This in effect lowers the maximum

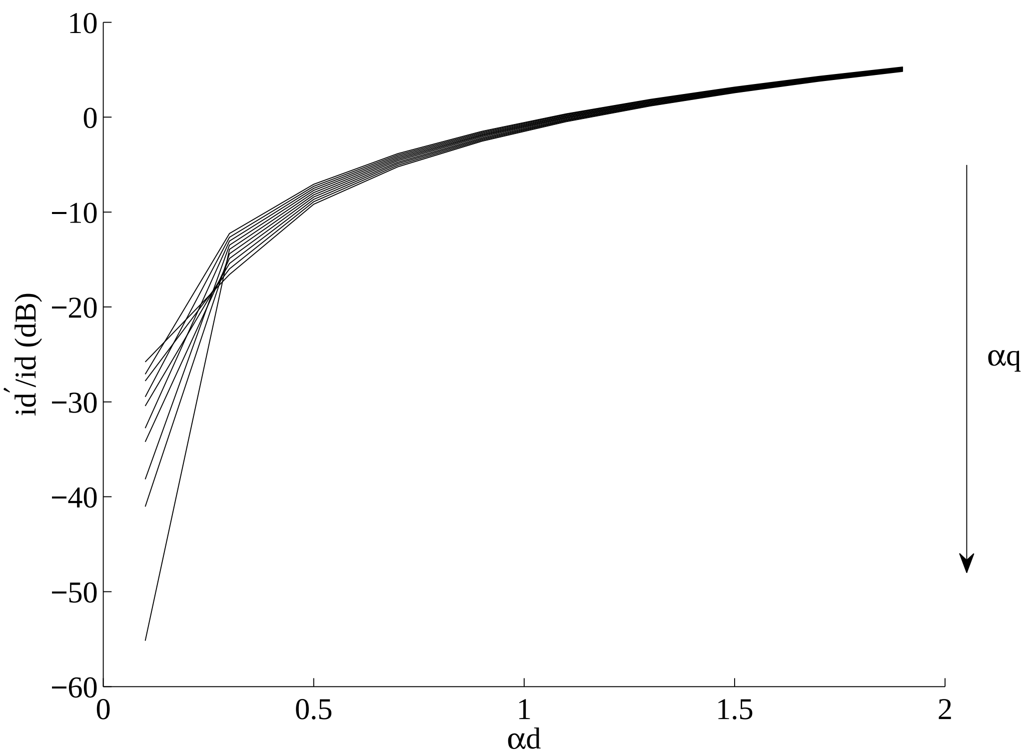

Figure 2.17: Change in the direct axis developed current with changing inductances

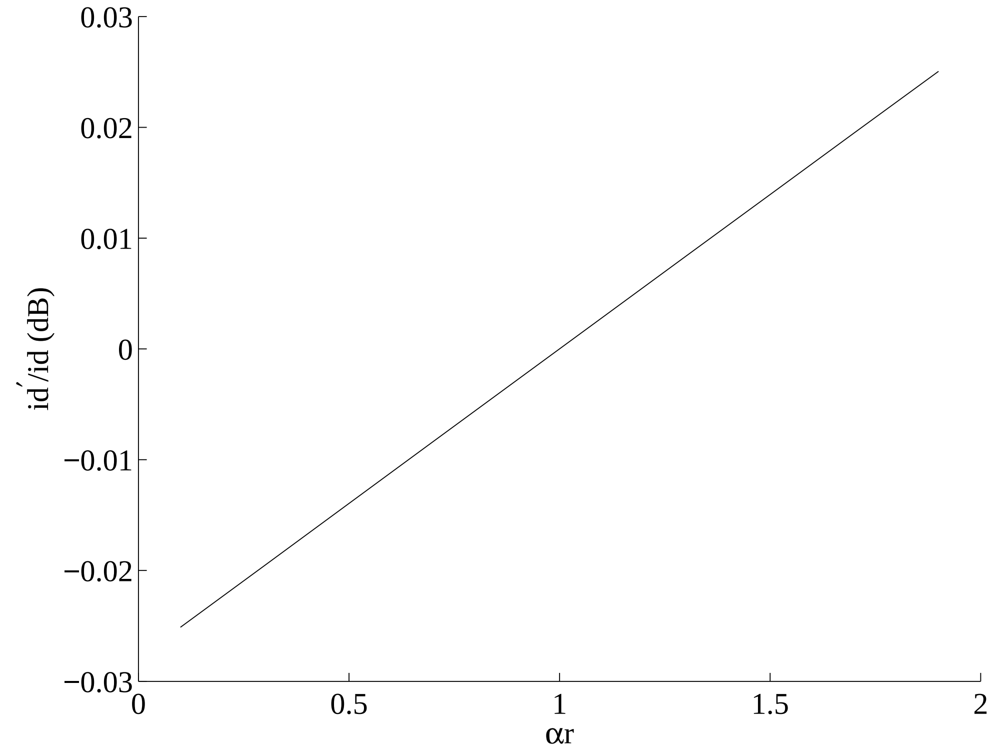

Figure 2.18: Change in the direct axis developed current with changing resistance and flux linkage due to the magnets

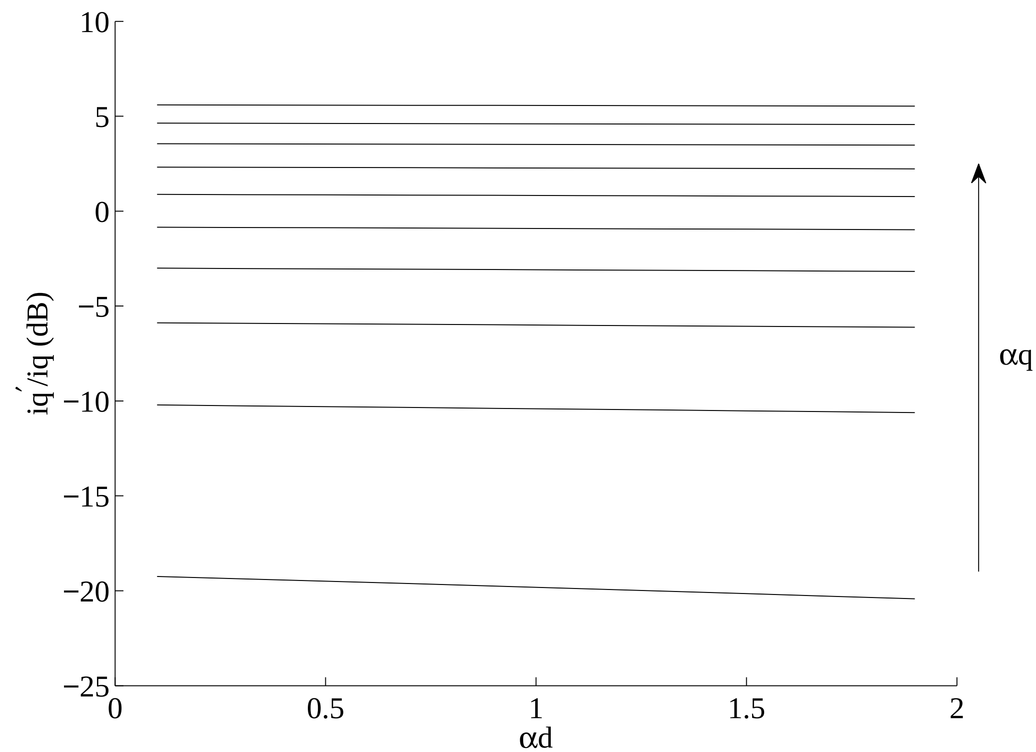

Figure 2.19: Change in the quadrature axis developed current with changing inductances

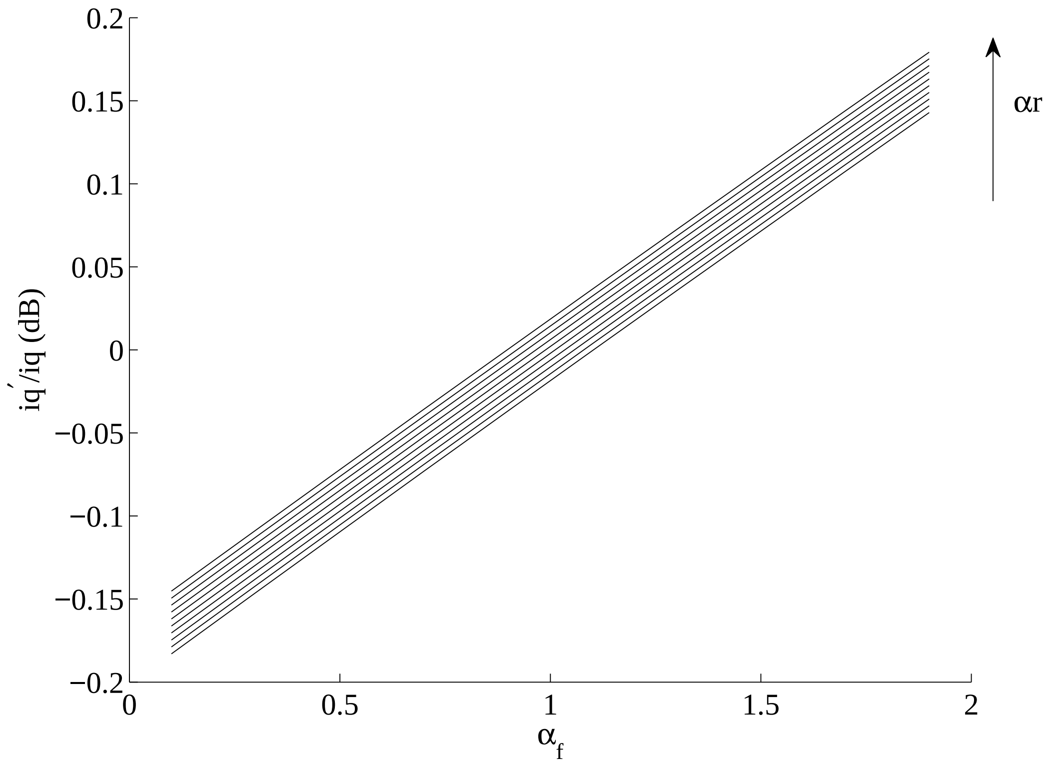

Figure 2.20: Change in the quadrature axis developed current with changing resistance and flux linkage due to the magnets

torque, as the controller will apply half of the current actually needed to give a given torque.

$$T = \frac{3}{4} P \lambda'_{af} i_{qs} \tag{2.43}$$

$$... = \frac{3}{4} P \alpha_f \lambda_{af} i_{qs} \tag{2.44}$$

In the salient case, the torque produced is due to both the magnets and the saliency. The magnet torque is affected in the same manner as the nonsalient case as α_f is changed in Fig. 2.21. The new analysis here is dealing with the change in direct and quadrature axis inductances. Clearly, both the direct and quadrature axis inductances have a large effect upon the torque as in Fig. 2.22. This makes their accurate determination during operating important.

$$T = \frac{3}{4} P[\lambda'_{af} + (L'_d - L'_q) i_{ds}] i_{qs} \tag{2.45}$$

$$... = \frac{3}{4} P[\alpha_f \lambda_{af} + (\alpha_d L_d - \alpha_q L_q) i_{ds}] i_{qs} \tag{2.46}$$

Rather than building a controller with inductances, creating one with flux linkages has its advantages. These advantages are apparent when one tries to find the inductance in either axis with little current present. The inductance will be quite large with a small current measuring error, as the flux derived in the characterization section 2.1.2 with equation (2.19) is divided by this current. Thus, looking at sensitivity of the torque equation with respect to the flux dependant torque equation will be of some use. These equations are given in (2.47) and (2.48). The effect that errors in the known fluxes can be seen in Fig. 2.23, where both flux errors have a large effect upon the developed torque. The large effect can be understood

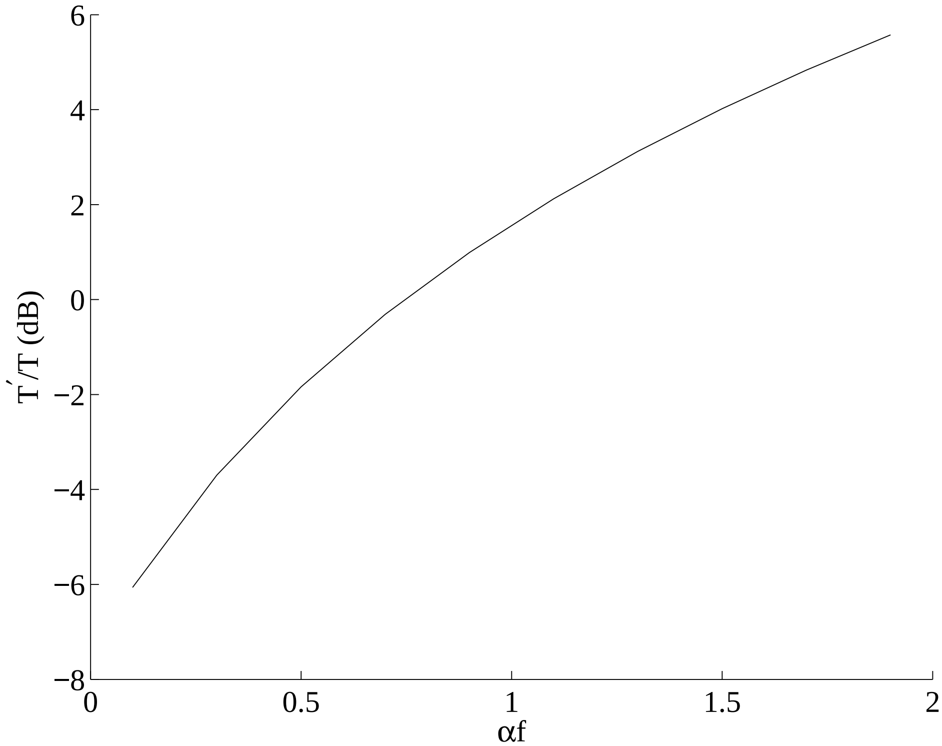

Figure 2.21: Change in the torque with changing flux linkage due to the magnets

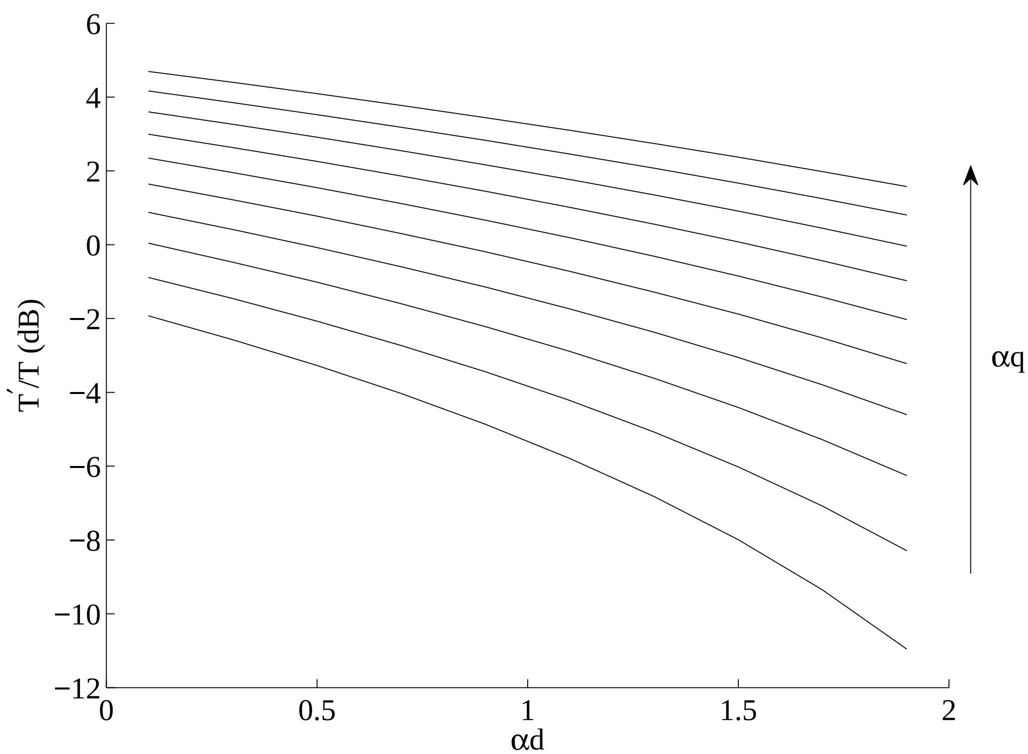

Figure 2.22: Change in the torque with changing direct and quadrature axis inductance

in that changing the flux indicates an error in the inductance/current product.

$$T = \frac{3}{4}P\left[\lambda_d' i_{qs} - \lambda_q' i_{ds}\right] \tag{2.47}$$

$$... = \frac{3}{4}P\left[\alpha_{fd}\lambda_d i_q - \alpha_{fq}\lambda_q i_d\right] \tag{2.48}$$

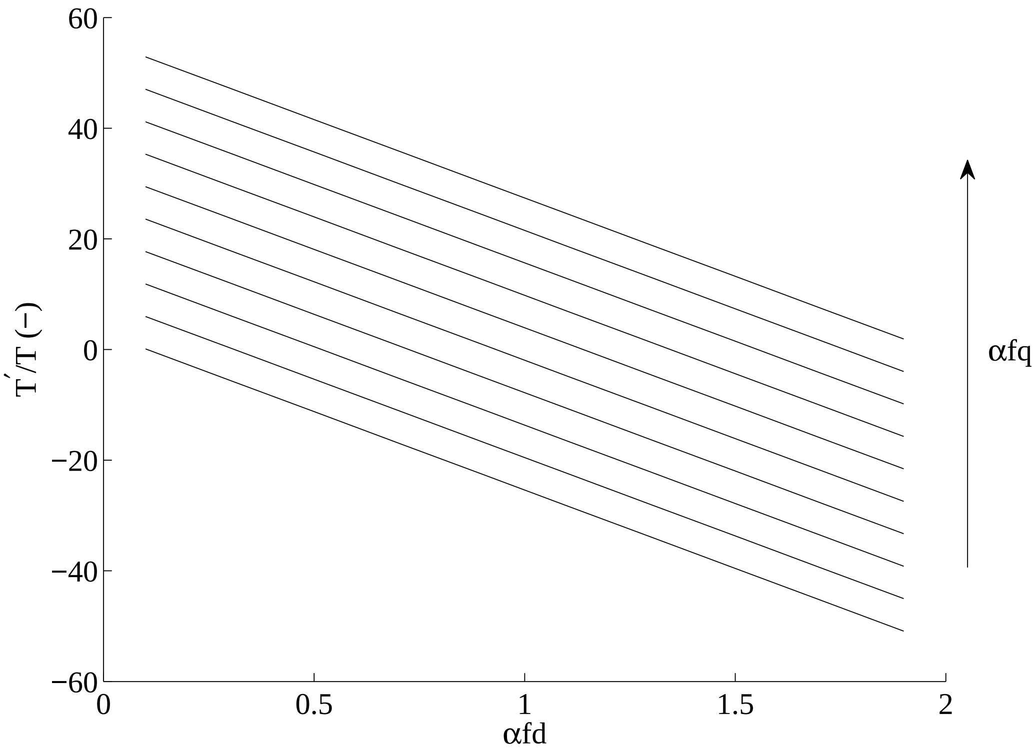

Figure 2.23: Change in the torque with changing direct and quadrature axis flux linkages

In the case of the nonsalient voltage limit circle equations in (2.49) and (2.50), the effect of inductance error upon the controller is seen in the change in the radius of the voltage circle. If α_s is 0.5, the radius of the voltage circle is doubled, which allows the controller to operate outside of its actual voltage limits. This can destroy the machine or prevent normal operation, and thus care should be taken to allow for DC link voltage margin that allows for some change in the inductance while keeping below the voltage limits. If α_s is 2, the voltage circle will shrink to half of its normal value, and merely artificially limit the operating range of the machine.

$$(i_{ds} + i_{sc})^2 + i_{qs}^2 = \frac{V_{max}}{\omega_e L'_s} \tag{2.49}$$

$$... = \frac{V_{max}}{\omega_e \alpha_s L_s} \tag{2.50}$$

$$\frac{(i_{ds} + i_{sc})^2}{(\frac{V_{max}}{\omega_e L'_d})^2} + \frac{(i_{qs})^2}{(\frac{V_{max}}{\omega_e L'_q})^2} = 1^2 \tag{2.51}$$

$$\frac{(i_{ds} + i_{sc})^2}{(\frac{V_{max}}{\omega_e \alpha_d L_d})^2} + \frac{(i_{qs})^2}{(\frac{V_{max}}{\omega_e \alpha_q L_q})^2} = 1^2 \tag{2.52}$$

In the case of the salient voltage limit ellipse equation simplified to show the radii in (2.52), the effect of errors in both inductances upon the controller is seen in the change in the radii of the voltage ellipse in Fig. 2.24. If α_d is 0.5, the horizontal radius of the ellipse will double, and again assume operation is possible outside of the actual voltage constrains. The machine will either not operate, or in the extreme case, be damaged. The same is for an α_d of 0.5, which would double the vertical radius, and allow for operation outside the machine voltage ratings. Again in the salient case, care should be taken to allow to allow for a DC link voltage margin slightly higher than what the controller is designed for to allow for an unmodeled decreased inductance value. If either α_d or α_q were to double, the range would merely be reduced. The reduction in operating range reduces the utility of the machine, and thus the inductances should be known accurately for effective machine use. Further, this exemplifies the need for having a model including saturation during controller development.

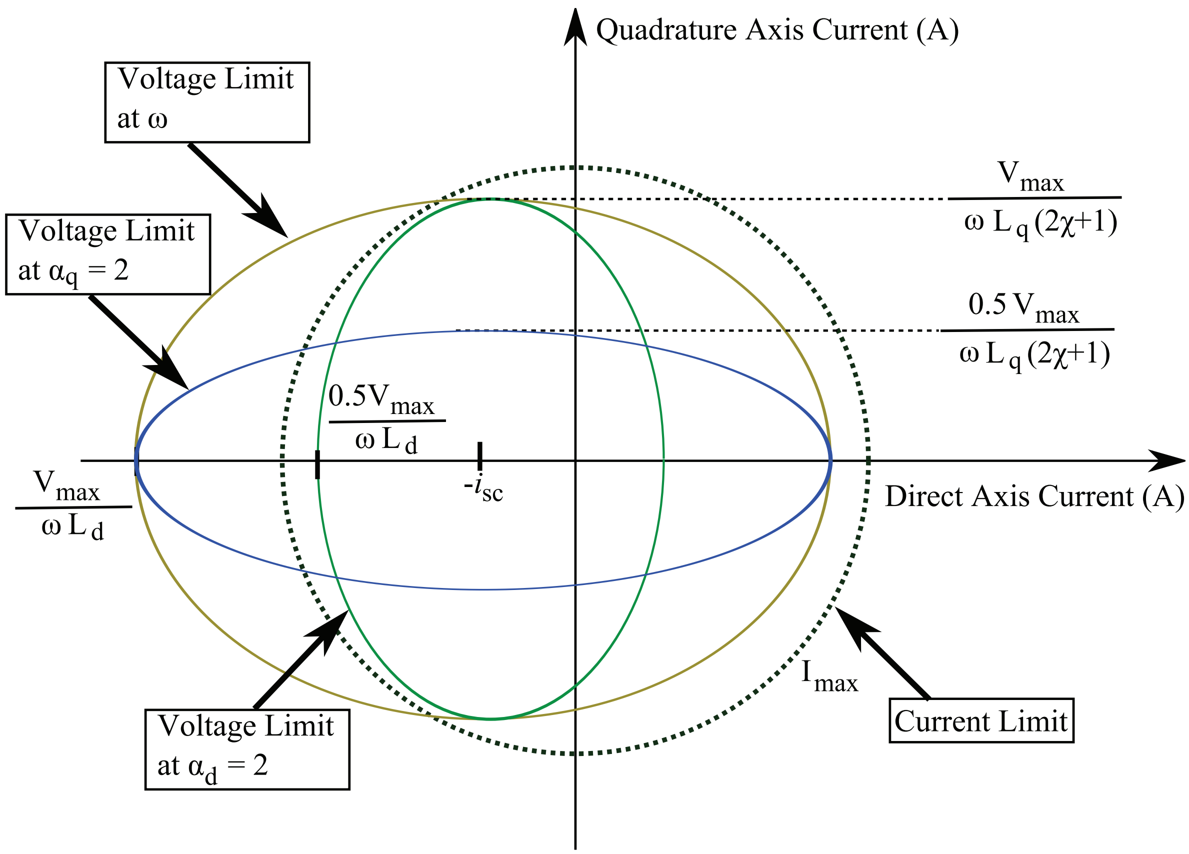

Figure 2.24: Plots for the changes in voltage ellipse due to parameter changes

2.2.3 Quantification of Parametric Error

A standardized technique must be found in order to make the relationship between parametric error and performance error clear. The parameters and performance measures have been clearly defined as tools for controller operation evaluation. Comparing the 'output', the variation in performance with the 'input' variation in the parameter which led to this error is the clearest measure possible. In order to experimentally determine the effect of parametric error, an error is induced in the controller while the machine remains unchanged. This simple error is given in [1] by the relationship in equation (2.53). The parameter quantity is given by ξ and the error induced in it is $\delta\xi$.

$$\xi_{error} = \xi(1 - \frac{error\%}{100\%}) \tag{2.53}$$

Once the error has been introduced and the controller has been modified with the erroneous parameters, the machine is operated from standstill to an operating point and the output performance is measured. The performance measure is given as P and the change in performance is δP. The ratio of the normalized change in performance to the normalized change in the parameter is defined as the sensitivity in equation (2.56).

$$\Delta_{\xi \to P} = \frac{\frac{\delta P}{P}}{\frac{\delta\xi}{\xi}} \tag{2.54}$$

$$\delta P = P_{actual} - P_{error} \tag{2.55}$$

$$\delta\xi = \xi_{actual} - \xi_{error} \tag{2.56}$$

This relationship gives a simple, quick, standardized way of measuring the effect that an error in a parameter has upon the output performance.

In the case of the dynamic performance of a machine, numerous dynamic performance measures can be used. These parameters represent the operation of the machine in the transient as the machine transitions to the steady-state. The parameter and its error are again used, but to distinguish the dynamic performance from the power performance, S and its difference from the original δS are used. This new relationship gives the effect of a change in a parameter upon the output performance of operation, such as a change in inductance's effect on the time to reach the steady-state torque. This relationship is given in equation

(2.59).

$$\Delta_{\xi \to S} = \frac{\frac{\delta S}{S}}{\frac{\delta \xi}{\xi}} \tag{2.57}$$

$$\delta S = S_{actual} - S_{error} \tag{2.58}$$

$$\tag{2.59}$$

2.3 Sensitivity Analysis Procedure

As the goal of this thesis is to find the effect that multiple parameter errors have, the process of computing the sensitivity with performance measurements of a machine or controller with erroneous parameters must be repeated multiple times. This process of computing the sensitivity from an erroneous controller is defined as a sensitivity set. A set results in a sensitivity from a specific parameter error to a specific performance outcome. This sensitivity set involves a process of characterization, controller development, performance measurement, and sensitivity calculation. This procedure is standardized and repeated multiple times to result in an array of sensitivity measures; various parameters and performance measures are used. Fig. 2.25 shows this procedure for one such sensitivity set.

The sensitivity procedure is summarized in Fig. 2.25. The first step is to define the machine model and the typically fixed parameters which are used in the machine model. The second step is then to extract these parameters using a characterization procedure. Then one controller with accurate parameters and another with parameters which have errors introduced in them is used to control the machine. The performance is measured and compared by calculating the sensitivity.

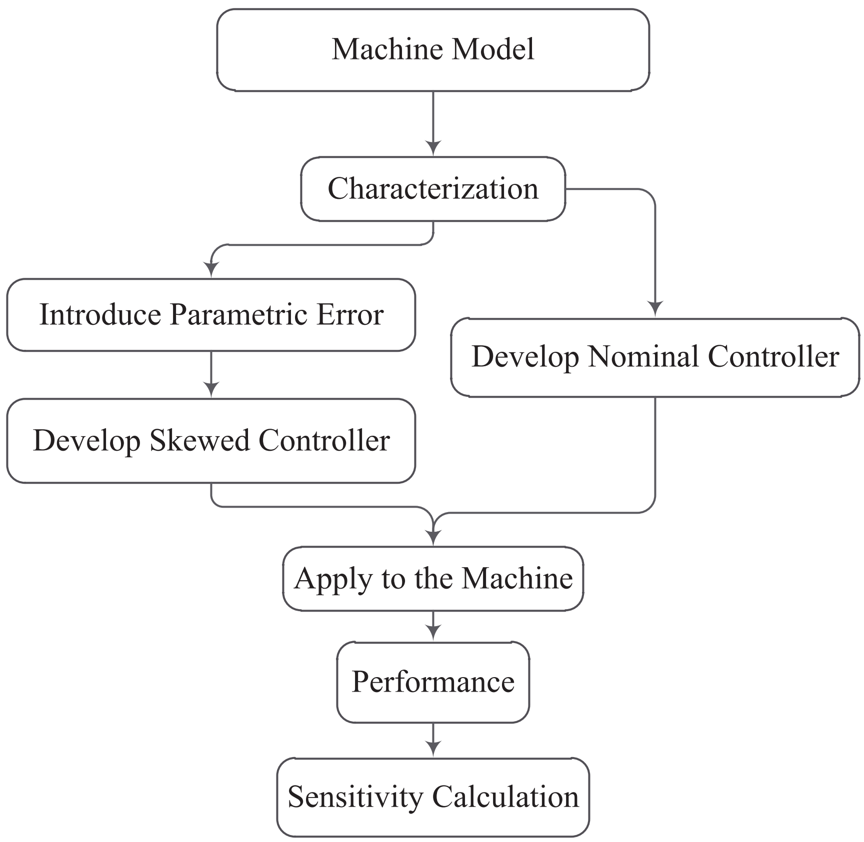

Figure 2.25: Flowchart of the procedure to determine sensitivity set

Chapter 3

Experimental and Simulation Results

3.1 Experimental Characterization Procedure

The foremost goal of experimental and FEA is to verify assumptions made in the analysis. The analysis discussed shows that it is possible to evaluate parametric sensitivity. The FEM verifies that the analysis holds with an actual machine model. The experimental work proves both the analysis and FEA, demonstrating that the work is practical. FEA and Experimental work are all done to verify the predicted results.

Overall, for data acquisition, the voltages, currents, torque, speed, and position are recorded. The appropriate quantities are then converted from their line-to-line values in the case of voltage to the phase voltage in equation (3.1). The phase voltages are found, then transformed to the rotor frame of reference by the relationship in equation (3.2), the opposite of the transformation discussed in section 2.1 with the transformation matrix of equation (2.4).

$$\begin{aligned} V_a &= \tfrac{2}{3}V_{ab} + \tfrac{1}{3}V_{bc} \\ V_b &= -V_{ab} + V_a \\ V_c &= -V_{bc} + V_b \end{aligned} \tag{3.1}$$

$$\begin{bmatrix} x_{qs}^r \\ x_{ds}^r \\ x_0 \end{bmatrix} = \begin{bmatrix} T_{abc} \end{bmatrix} \begin{bmatrix} x_{as} \\ x_{bs} \\ x_{cs} \end{bmatrix} \tag{3.2}$$

3.1.1 Characterization Procedure

3.1.1.1 Open Circuit Testing

The back-EMF is found by spinning the machine which receives a speed command, having removed the inverter connections from the second machine, or the one being characterized, and only measuring its terminal voltage. In order to characterize it, the machine must be appropriately oriented to apply current aligned with the flux, or of any angle beyond this. The rotor alignment is similar to [7], oriented to the positive peak of the back-EMF. In Fig. 3.1 the alignment is displayed with respect to the mechanical position as well as the measured back-EMF. This is from the acquired data and is for clarity. Thus, with the characterized machine being open-circuited, the machine equations simplify to (2.14) and (2.15), and are repeated in equation set (3.1). The voltage can then be transformed into the rotor frame of reference. Once in the rotor frame of reference, the d-component of the back-EMF should be zero, whereas the q component contains the constant value which is the back-EMF if the machine is properly aligned.

For the measurement of this λ_{af}, the rotor must be spun stably at a constant velocity while the voltage is measured. From this voltage the BEMF is determined with the equations

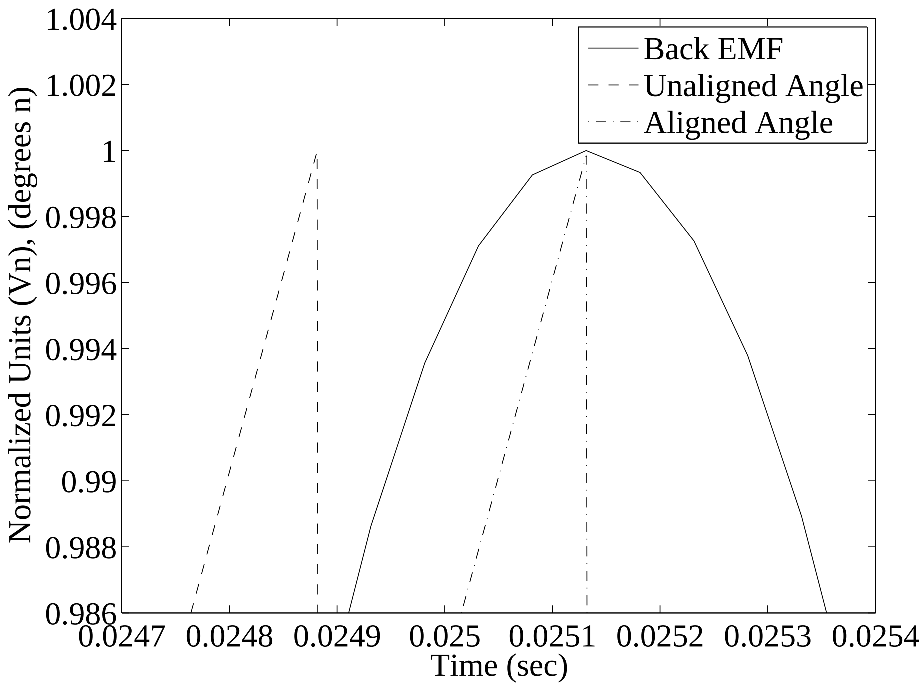

Figure 3.1: The angle offset plot used to first find angle offset, subtract this from the angle to achieve the angle aligned to the positive back-EMF peak

in (3.3).

$$\begin{aligned} v_{qs} &= \omega_r \lambda_{af} \\ v_{ds} &= 0 \end{aligned} \tag{3.3}$$

In addition to determining the alignment with respect to rotor position and back-EMF from these voltage measurements, the number pole pairs can be determined by plotting the phase voltage. The number of complete back-EMF cycles in one mechanical revolution defines the number of pole pairs.

3.1.1.2 Phase Resistance

In order to determine the phase resistance, an elementary DC test is used which is performed with the setup in Fig. 3.2 including two phases of the machine, a voltage transducer, and a DC supply with controllable current and voltage limit. From this test, a voltage and current will be derived. Using these two quantities, the resistance can be calculated with the equation in (2.13). Note that the resistance measured is twice that of the phase resistance.

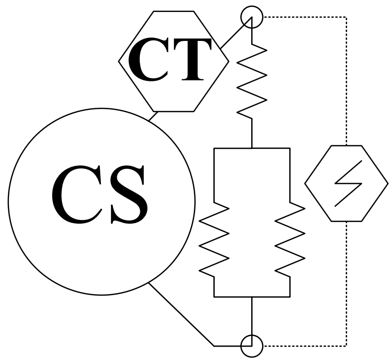

Figure 3.2: DC test for phase resistance

3.1.1.3 Flux linkages

In this section, the flux linkages for all possible currents are determined. The machine being characterized must be connected to the inverter, and without flux linkage knowledge, a simple controller must be developed. This controller discussed earlier will take the form of Fig. 2.5.

In this, a direct and quadrature axis current command is given, and if the gains of the PI controllers are chosen properly, the machine will attain these in reasonable time. A current angle and magnitude are defined and applied, resulting in the direct and quadrature axis currents as in equation (3.4).

$$\begin{aligned} i_{ds} &= |I_s| \cos \delta \\ i_{qs} &= |I_s| \sin \delta \end{aligned} \tag{3.4}$$

In characterizing, commands for as many operating points are given as should be expected during operation. Typically this means giving current magnitude commands ranging from

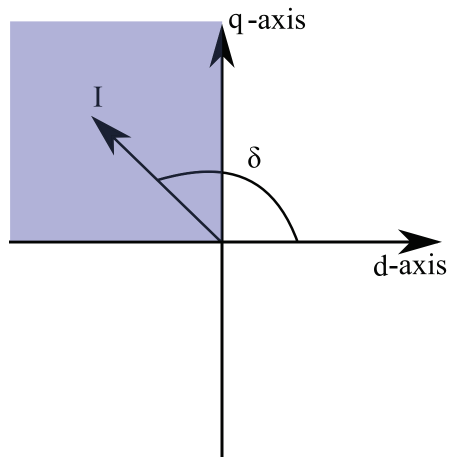

Figure 3.3: Current vector range applied during characterization

no current to the maximum current rating of the machine. For each of these magnitudes, the angle should be varied from the point of maximum torque and no flux weakening, to the point of maximum flux weakening and no torque. An example of this is given for the entire second quadrant in Fig. 3.3. Knowing the magnitude variation is straightforward, but knowing the angle variation is not. Recall the voltage and flux relationship in equation (3.5).

$$V_A = \frac{d\lambda_A}{dt} \tag{3.5}$$

The back-EMF is the voltage induced by the magnet flux. For alignment, the back-EMF can be visualized as a cosine wave with zero phase. The vector is represented in Fig. 3.4 diagram showing the magnetic axes with a fictitious one pole pair rotor. This means that the integral of a cosine wave will result in the flux linkage by phase A. In order to weaken this field a negative sine must be applied for phase A. From the defined transformation, an angle of $\delta = 0$ for any magnitude value gives a positive direct axis current, and a sine wave as the voltage command. This means that an angle of $\delta = 0$ results in the maximal flux strengthening. Thus, to operate in the flux weakening range with positive torque which the machine will most likely be operated in, the angle δ should range from 90 °through 180 °. A plot showing the relationship between phase A quantities with repect to rotor position is given in Fig. 3.5.

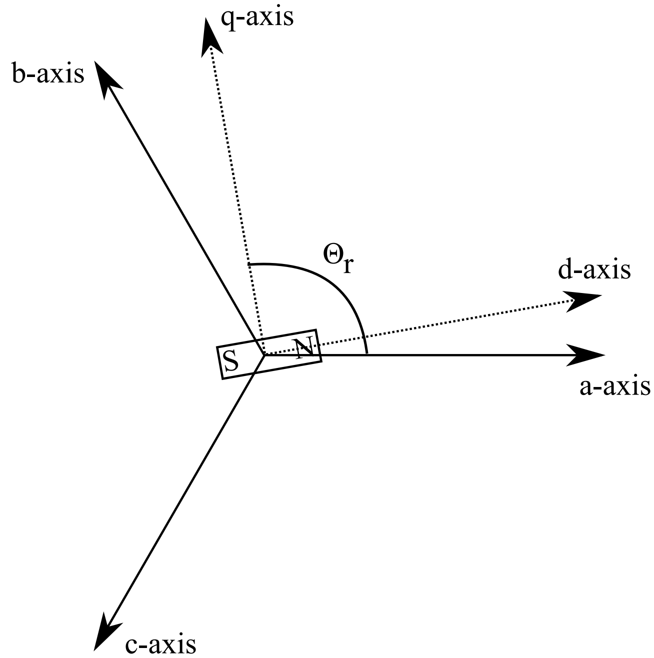

Figure 3.4: Vector diagram including fictitious rotor magnet

$$\lambda_A = \int V_A \, \mathrm{d}x \tag{3.6}$$

Thus to gather the flux linkage data, a large number of magnitudes and angles should be used spanning the range of operation. For each, the magnitude, angle, torque, speed, as well as the voltage and current waveforms were recorded. Using the transformation to the rotor frame of reference, the rotor aligned values are found, and should be, like the speed, constant. This information will be used to find the flux linkages if operation at constant speed and current is maintained. This is necessary as the machine model simplifies to equation (3.7),

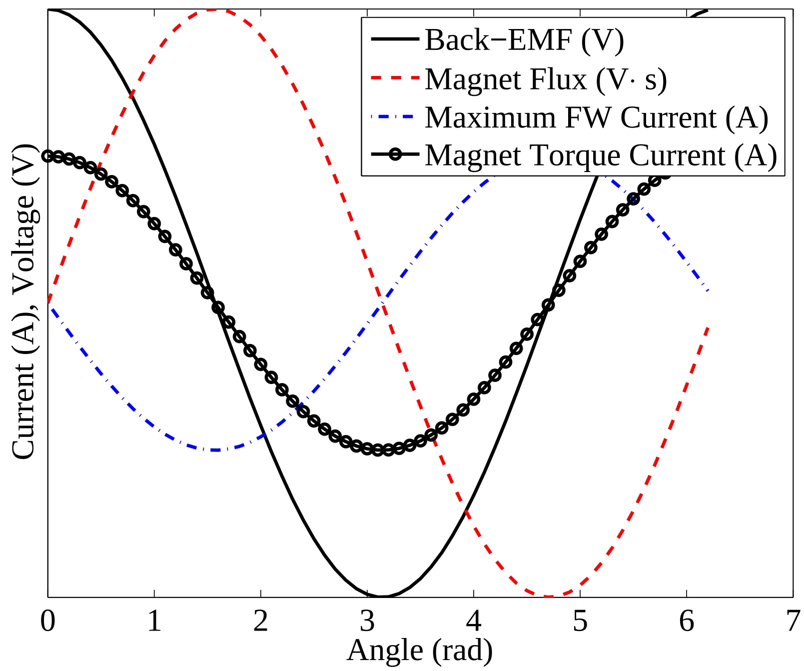

Figure 3.5: Sinusoids for the phase A quantities

repeated from section 2.1.2.

$$\begin{aligned} \lambda_q &= \frac{-v_{ds}+i_{ds}R_s}{\omega_e} \\ \lambda_d &= \frac{v_{qs}-i_{qs}R_s}{\omega_e} \end{aligned} \tag{3.7}$$

The flux linkages are found from this, and this procedure should be repeated for every operating point of interest, so that that the flux linkages are found from magnitudes ranging from zero to $|I_{max}|$ and from angles ranging from 90° to 180°. It was shown before that the flux linkage is found with integration of the voltage, which would of course have the problems introduced by integration; in this circumstance as the flux linkages are calculated without integration these problems are avoided. The fluxes can then be used to find the inductances and transient inductances. If the data is noisy, some post processing may be helpful.

3.1.2 Flux Linkage Data processing

For each of the voltage and current data, a simple filter can remove switching noise and other harmonics, so that the fundamental can be derived, being the main torque producing component. A third order Butterworth filter is used to filter the data in this paper. Using MATLAB, a digital filter is created, which is used to extract the fundamental from all of the noisy waveforms. As the $filtfilt()$ function is used in MATLAB, zero phase delay is achieved, but the magnitude attenuation must be determined using the bode function as the signal is attenuated by the square of the filter magnitude at the appropriate frequency. Note that the $filtfilt()$ function determines the phase delay for the resulting frequencies, and uses this to compensate and thus achieves zero phase delay. In order to determine the exact frequency, the Fast Fourier Transform is performed on the filtered waveform, and this frequency is used to determine the magnitude attenuation. Using this method, the waveform in Fig. 3.6b can be achieved from Fig. 3.6a.

Once the fundamental can be derived, the d- and q- axis components can be derived in one of two ways: the Park's transformation or measurement at specific positions on the waveform. The Park's transform will give a constant direct and quadrature axis value, as it calculates at every angle. The phase A, B and C values as well as position are read and transformed with equation (3.2). This is one method, but another can be performed by simply comparing the phase A voltage or current with the position. In Fig. 3.7, the back-EMF compared to the phase angle. The value when position is zero degrees gives the direct axis quantity, while the value at position of ninety degrees gives the quadrature axis quantity. It is clear that this will not give you the direct and quadrature axis values at all times, just those that coincide with the angle at 0 $^\circ$or 90 $^\circ$.

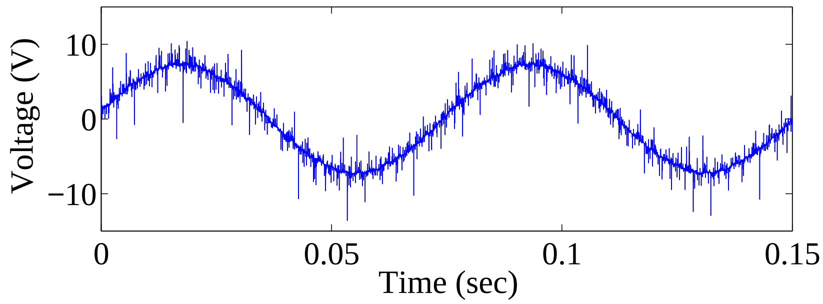

(a) Unfiltered Back EMF

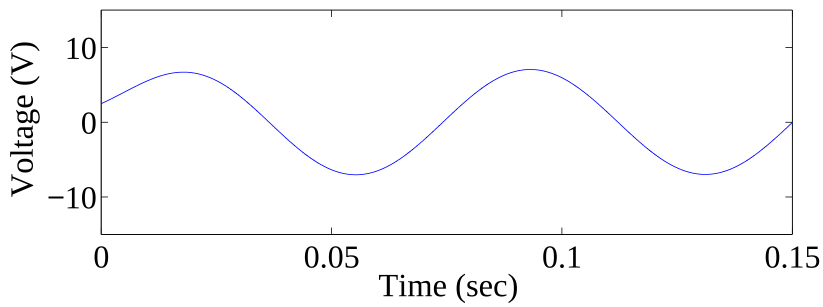

(b) Filtered Back EMF

Figure 3.6: Demonstration of filtering to produce clearer waveforms

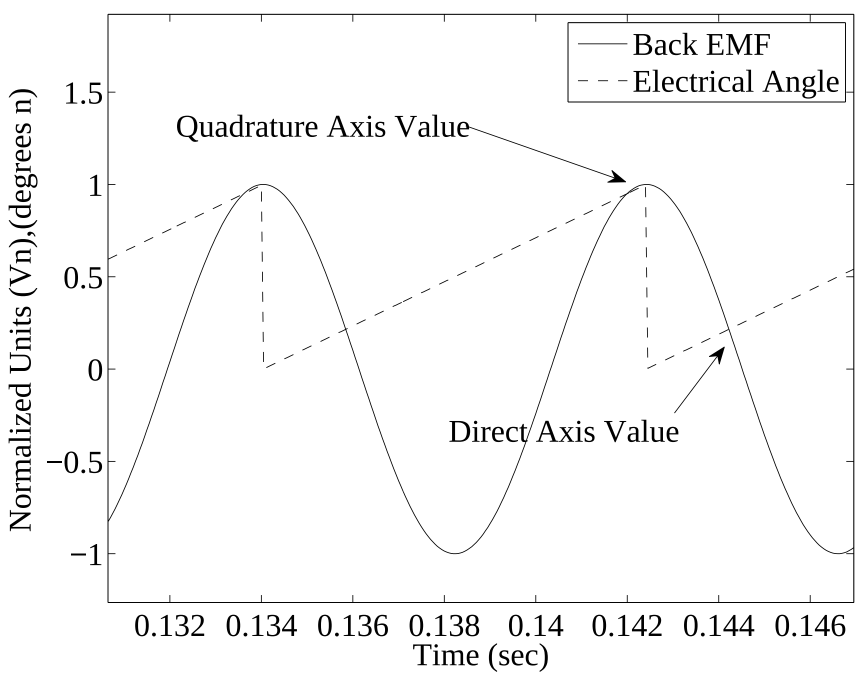

Figure 3.7: Plotting the phase A voltage with back-EMF to find d- and q- axis values

3.2 SPM Machine Current Controller Sensitivity

3.2.1 Method of Characterizing SPM and IPM machines

Note that in the model, the main parameters which must be found are the phase resistance, the flux linkage constant due to the magnets, and the flux linkages at each operating point. In order to do this characterization for the SPM machine a characterizing system which utilizes two identical machines, each controlled by an inverter is used. In one inverter, a DSP, the Texas Instruments fixed point DSP TMS320F2810 is used to control the speed of one machine, with a simple PI controller system, from commands given through the Controller Area Network by an external computer controlled by a Labview interface. Another inverter containing the Texas Instruments floating point DSP TMS320F28335, which controls a machine mechanically attached to the shaft of the other, takes current commands, including magnitude and angle from a computer, through the controller area network.

For each machine, two line-to-line voltages and two phase currents are measured for data acquisition by voltage sensors and current transducers (CT), respectively. Position is read with an encoder from both inverters, which is used to measure position and speed. A torque sensor, which connects to the shafts of both machines, measures the torque applied between the machines. This data acquisition is performed by a Labview developed data acquisition system, which reads inputs through two National Instruments Data Acquisition (DAQ) cards. The general machine system is shown in Fig. 3.8, including all sensors.

The sensitivity measure in section 2.2.3 is applied to the machine in simulation, found to have the parameters as in Table (3.1). Note that the inductance is not current dependant, but chosen to be constant due to a low degree of saturation. The speed is not the rated machine value, but the machine operating condition for the tests performed. Note that

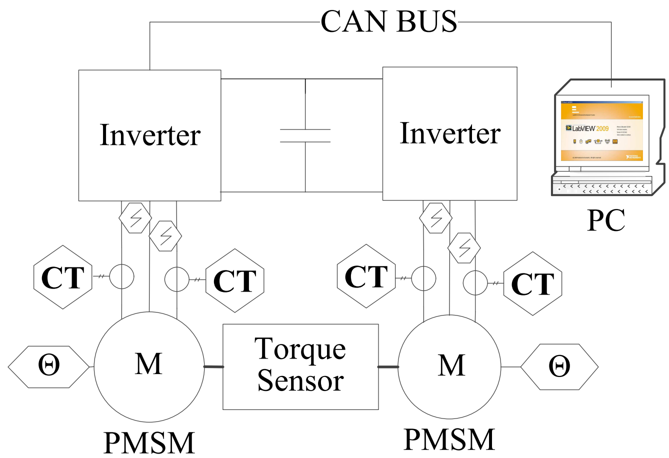

Figure 3.8: Physical test setup for SPM machine characterization with inverters, machines and sensors

only one inductance is given. This is due to the fact that the machine has surface mounted magnets, which should then not result in a large of inductance variation by axis.

Table 3.1: Characteristics of surface mounted permanent magnet machine

27.5 $(m\Omega)$	Resistance of One Phase
30	Number of Poles
0.0862 $(V \cdot s)$	Flux Linkage due to Rotor Magnets
3.585 (mH)	Total Inductance
80 $\left(\frac{rad}{sec}\right)$	Electrical speed of machine

Now that the sensitivity measurements have been defined, simulations will be performed while varying each parameter. For each variation of parameter, the output performance is measured: dynamic, power, efficiency, and torque performance measurements. The first table shows the performance data: the torque, power and efficiency readings. The second shows the effect of parametric errors on dynamic performance data including rise time, settling time and steady state error. Finally, the last table shows the sensitivity, calculated with the method discussed in the last section. Note that in each instance an error is introduced into one of the machine parameters in the controller. For instance in Table (3.2) the first line is the result of no error, whereas the second line is the result of halving the phase resistance. Only one parameter is given an error at each test, and each is halved in the respective test.

Table 3.2: Table showing the various output metrics with respect to varying parameters

P	$Error\ (\%)$	$Torque\ (N \cdot m)$	$Power\ (W)$	$\eta\ (\%)$
$Nom.$	0%	97.776	4991.88	97.94%
R_s	50%	97.77	4991.69	97.93%
L_s	50%	97.57	4981.88	97.93%
λ_{af}	50%	97.6	4982.62	97.94%

Table 3.3: Table showing the various dynamic response metrics with respect to varying parameters

S	Error (%)	$T_r\ (sec)$	$T_s\ (sec)$	$e_{ss}\ (\%)$
$Nom.$	0%	$2.71e-4$	0.1003259	0%
R_s	50%	$1.27e-4$	0.1003258	-0.00383%
L_s	50%	$2.64e-4$	0.1003	0%
λ_{af}	50%	$2.6444e-4$	0.1003311	-0.18033%

Table 3.4: Table showing the sensitivity of output and dynamic response metrics with respect to varying parameters

$\Delta_{\xi \to S,P}$	R_s	L_s	λ_{af}
$T\ (N \cdot m)$	$70.09e-6$	$4.09e-3$	$3.62e-3$
$P\ (W)$	0.076e-3	4e-3	3.71e-3
$\eta\ (-)$	1.81e-5	9.22e-5	6.2e-5
$T_r\ (sec)$	1.06	4.7e-2	4.63e-2
$T_s\ (sec)$	2e-6	3.5e-4	1.05e-4
$x_{ss}\ (A)$	7.67e-5	0	3.61e-3

From the data shown, some observations are made as to the sensitivity effects of various machine parameters. The torque is most affected by errors in the inductance as well as flux linkage due to the magnets, being significantly larger than the other two. This is because the torque depends heavily upon the inductances and flux linkage due to magnets. Resistance is shown to have a much lesser effect upon the output. The power is most affected by the inductance since this affects the calculated voltage command and an almost negligible amount by the phase resistance. The rise time had a large sensitivity with respect to phase resistance since the voltage command is reduced for any speed whereas the other metrics are much less significant. In the case of settling time, only the phase resistance does not have a large effect, the others all had a fairly similar effect. Finally, the steady state error is affected by the flux linkage due to the magnets and inductance, so for instances where accurate current control is desired, these should be the most accurately determined parameters.

Beyond the simulations, an experiment was performed to prove this performance data. In order to gather data, the test machine is spun with another machine at constant speed while a 5 A quadrature axis current was applied to the test machine. The quadrature axis current command was then abruptly changed to 10 A, while the data acquisition measures all operating data. This was then used to gather the same data which was found during simulation. This experiment was repeated with the introduction of parametric error in the parameters during simulation. As with the simulation, the experimental data is used to generate sensitivity data. This data was given in Table (3.5). From the experimental data the flux linkage due to the magnets, much like the simulation, seems to have a large effect upon the output. This is also seen more so with the inductance variation, the sensitivity being higher especially in the case of steadystate error and other transient responses. The resistance has the least effect, which is also seen in the simulated data.

Table 3.5: Table showing the experimentally determined sensitivity to parametric error

$\Delta_{\xi \to S,P}$	R_s	L_s	λ_{af}
$T\ (N \cdot m)$	0.705	0.610	2.201
$P\ (W)$	0.785	0.695	1.811
$\eta\ (-)$	0.536	0.664	1.289
$T_r\ (sec)$	0.750	1.563	0.100
$T_s\ (sec)$	0.028	1.008	1.285
$x_{ss}\ (A)$	0.002	1.031	1.521

3.3 IPM Machine 1 Torque Controller Sensitivity Using FEA

3.3.1 Finite Element Analysis for Characterization

An IPM machine was modeled with the Flux2D software package, for use in the simulation of these machines. The designed finite element model is verified by conducting a back-EMF test as well as applying known currents to check whether the predicted torque is achieved. In addition to performance fidelity with the actual machine, the finite element model software allows us to apply currents and voltages by use of the controllers and measure all performance parameters.

3.3.2 Finite Element Model

A finite element model is sought to first prove the concepts of sensitivity, as it best approximates machine behavior outside of experimental work. The finite element model was constructed and given a mesh using the Flux2D finite element analysis software package. The simulation parameters are discussed here. Note that the general finite element model design is given in Fig. 3.9, where the colors define certain regions.

Table 3.6: Fig. 3.9 color legend

FEA Color Legend		
Other	Infinite Box	Black
Magnets	Magnets	Red
Windings	A+	Yellow
	A-	Black
	B+	Green
	B-	Red
	C+	Cyan
	C-	Blue
Iron	Stator	Fuchsia
	Rotor	Cyan
Air	Rotor	Black
	Stator	Blue
Airgap	Stator	Blue
	Rotor	Black

Note that in Table (3.6) the colors for the various regions in the FEM are given. As some are repeated, take note that the coils are the small rectangular regions within the mode, the large center black circle is the rotor air, the large black on the outside is the infinite box. The blue area just within the infinite box is the air surrounding the stator. The large cyan area with the magnets embedded is the rotor iron. The fuchsia area inside of the stator air is the stator iron.

The mesh and geometry for this finite element model is seen in Fig. 3.10. It is difficult to see the details of the mesh, so the mesh point information is given by Table (3.7).

A circuit must be coupled to this model, and from the winding diagrams the circuit in Fig. 3.11 corresponds to the machine. In Flux2D, the coil conductor lumped element defines the current through the appropriate coil conductor of the geometry. In this, each positive circuit element corresponds to the outward facing conductor in the geometry, while the negative circuit element corresponds to the inward facing conductor. Note that also the

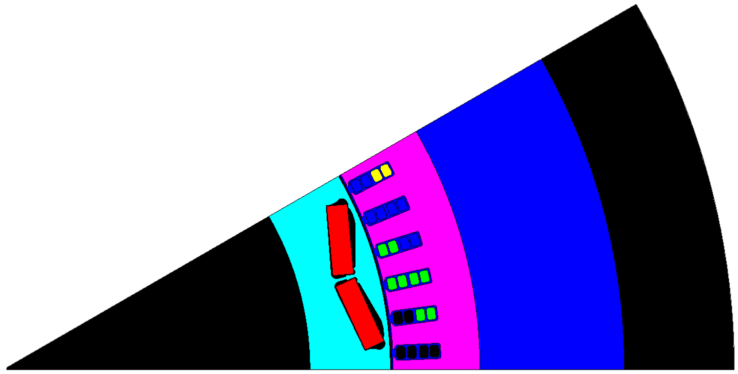

Figure 3.9: View of the partial Flux2D geometry finite element model

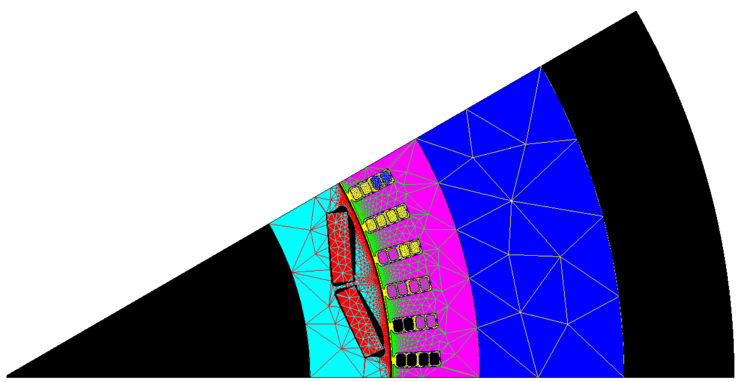

Figure 3.10: View of the partial Flux2D geometry finite element model with mesh

phase resistance and leakage inductance are included, determined from the Speed software package. Additionally, three AC voltage sources are shown, while in simulation either voltage or current may be used.

Table 3.7: Mesh point values for Fig. 3.10

FEA Mesh Values		
Large	Inner Rotor Iron Outer Stator Iron	15 (mm) 15 (mm)
Medium	Magnets Radial Outermost Slot	3 (mm) 3 (mm)
Small	Radial Innermost Magnet Other Slot	0.5 (mm) 0.5 (mm)
Airgap	Airgap	0.2 (mm)
Small Airgap	Airgap Midpoint	0.1 (mm)

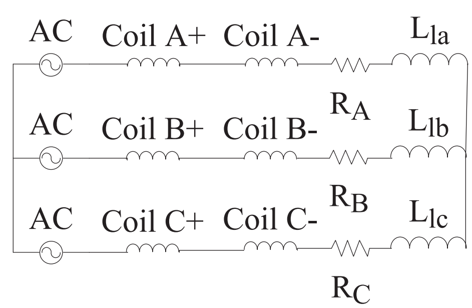

Figure 3.11: Circuit of the FEM

3.3.3 Finite Element Simulations

Using this circuit along with the FEM, certain scenarios are used for simulation of a healthy machine mimicking the performed experiments. The characterization imposes a constant speed of 2449 RPM, while applying a set DC quantity of either direct or quadrature axis current with a current source, and again measures all quantities. This is conducted for a time from 0 to 0.16 seconds in steps of 300 μsec and applies current from 0 to 350 A in steps of 35 A. The performance simulation applies currents to achieve a specified torque from the torque/speed to current lookup table while spinning the machine at 2449 RPM in order to generate a torque of 180 $\mathrm{N \cdot m}$. In experimentation: 166.6 $\mathrm{N \cdot m}$ is achieved, thus a torque error of 7.4% exists in simulation.)

The sensitivity measure in section 2.2.3 was applied to the IPM machine in the finite element analysis software package Flux2D, with the parameters in Table (3.8). Note that only the quadrature axis inductance is current dependent, as the self saturation of the quadrature axis is quite high. The flux with varying current was found and the inductance from this was used to calculate a family of torque/speed curves. The speed was not the rated machine value, but the machine operating condition for the tests performed. A torque/speed point taken from the torque/speed curve was used and the performance at this point was measured. This measurement was compared to the parametrically correct controller for torque and efficiency; this was used to determine the sensitivity.

Table 3.8: Characteristics of interior permanent magnet machine 1

29 $(m\Omega)$	Resistance of One Phase
12	Number of Poles
0.078 $(V \cdot s)$	Flux Linkage due to Rotor Magnets
$0.84 - 0.0016$ (mH)	Quadrature Axis Inductance
0.243 (mH)	Direct Axis Inductance
1539 $\left(\frac{rad}{sec}\right)$	Electrical speed of machine

The flux was found as discussed for the nominal machine to be used as a starting point. The flux curves depending on both the direct and quadrature axis current are shown in Figs. 3.12 and 3.13. Note that the quadrature axis flux is heavily dependent upon the current, especially at the high values of quadrature axis current, where the flux saturates heavily. Some cross saturation is evident from the flux changing for different values of direct axis current. Also note that the direct axis flux and inductance is much less effected by saturation, but some effect can be seen. In the nominal controller, the quadrature inductance is approximated by a linear function which best represents the inductance found from these

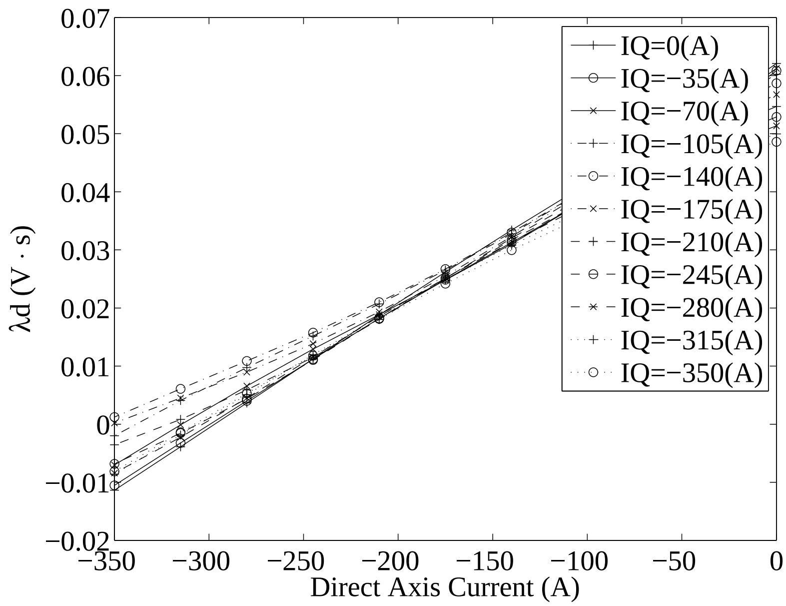

Figure 3.12: Current dependency of the direct axis flux linkage

flux curves. The direct axis inductance is assumed to be constant.

The parameters were used to find torque/speed controllers for the machine. This controller is represented in the form of torque/speed curves which have the current values needed for each operating point. The relationship between torque/speed and D/Q current was found and used to operate the machine. The parameters had error introduced into them, the controller recalculated, and operated at this point once more. The torque speed plots are shown in Fig. 3.14. The torque speed curves change only due to the change in the known machine parameters. Changing the parameters will only change the model and controller for the model, not the actual machine. Neglecting saturation, the maximum torque below base speed is high, due to the assumption that high current will not saturate the quadrature axis, and thus the saliency torque will always remain at its highest level. Like in previous results, the resistance does not change the controller much at all. As was seen before, an error in λ_{af} has a large effect upon the torque; when this is assumed to be half, the magnetic torque expected is halved. The torque below base speed is not halved because a great deal of torque

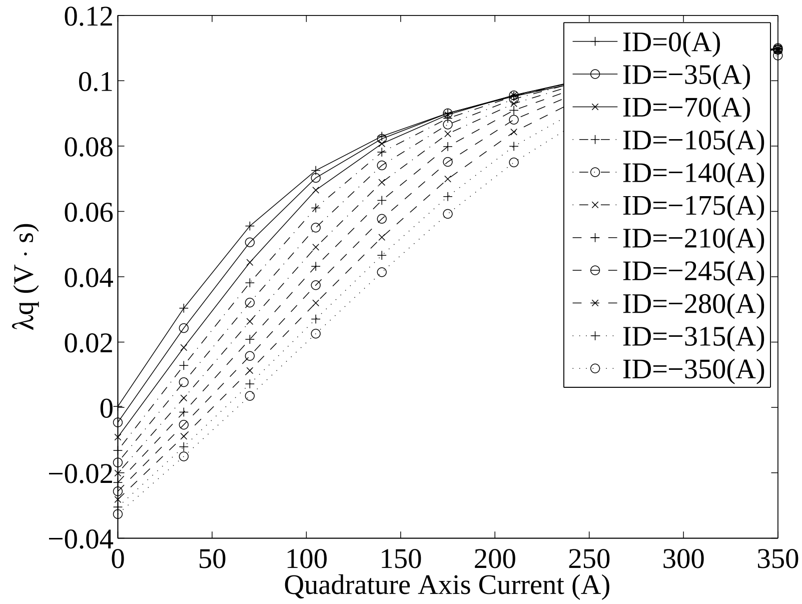

Figure 3.13: Current dependency of the quadrature axis flux linkage

in an IPM machine comes from saliency. The base speed increases because the voltage the magnets induce in the stator is assumed to be halved. The torque expected when there is error in L_q is halved because the saliency torque is then assumed to be much less. Typically, the quadrature axis inductance is twice that of the direct axis inductance; when the quadrature axis is halved, the saliency torque is assumed to be gone. The base speed increases in part because a halving of the inductance reduces the voltage induced in the direct axis when quadrature current is present. This means that field weakening is not required until higher direct and quadrature axis currents are needed. If the direct axis inductance is halved, the torque increases compared to the nominal because more saliency torque is assumed to be developed. The maximum speed decrease can be seen in the maximum speed equation (3.10), assuming all of the current applied contributes to field weakening. When the direct axis inductance is reduced, so is the maximum speed attainable with maximum current.

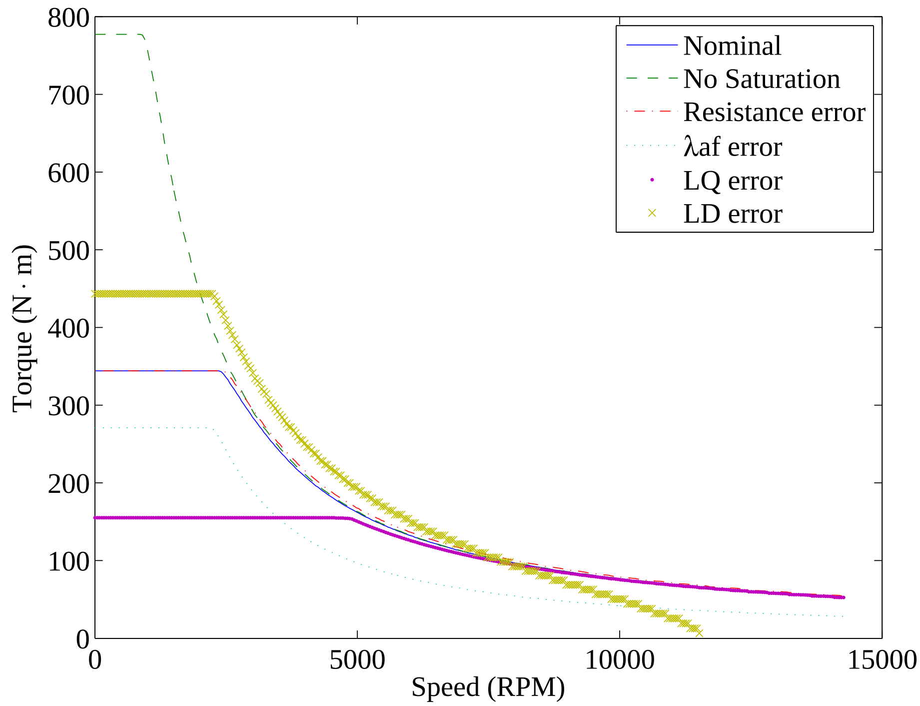

Figure 3.14: All torque and speed curves

$$v_s^2 = v_{ds}^2 + v_{qs}^2 \tag{3.8}$$

$$... = (i_{ds}R_s)^2 + (\omega_{max}\lambda_{af} + \omega_{max}L_d i_{ds})^2 \tag{3.9}$$

$$\omega_{max} = \frac{v_s^2 - i_{ds}^2 R_s^2}{\lambda_{af}^2 + L_d^2 i_{ds}^2 + 2\lambda_{af} L_d i_{ds}} \tag{3.10}$$

With the parametric sensitivity procedure, the sensitivity is calculated for the effect of various parameters upon output performance and shown in Table (3.9). The results agree with that previously seen in the nonsalient machine. The inductance here has a larger effect, especially the quadrature inductance, as this has an effect on saliency torque. The torque change is reflected in both the power and efficiency, too. The resistance has a small effect as before as does the direct axis inductance. The flux linkage due to the magnets is seen to have a large effect, too as this has a large effect upon the magnet torque. A new phenomenon is seen in this case compared to the nonsalient machine case. The sensitivity of direct axis current to quadrature axis inductance is very high. This is due to the dependence of the operating point on the level of saliency from equation (2.32). With an error in this quadrature axis inductance, the saliency is assumed to be reduced and thus the saliency torque. With less dependence on saliency torque, direct axis current is not important for torque, only flux control.

Table 3.9: Table showing the finite element determined sensitivity to parametric error

$\Delta_{\xi \to P}$	λ_{af}	L_d	L_q	R_s
$T\ (N \cdot m)$	0.8765	0.1887	1.5715	0.0410
$\eta\ (-)$	0.1226	0.0049	0.1785	0.0292
$P_{mech}\ (W)$	0.8765	0.1887	1.5715	0.0410
$P_{elec}\ (W)$	1.0646	0.1932	1.9198	0.0713
$I_D\ (A)$	2.300	0.3500	2.600	0.1500
$I_Q\ (A)$	0.1739	0.0217	0.6957	0.2391

3.4 IPM Machine 2 Experimental and Simulation Results

Accurate performance measurement and controllers rely on accurate characterization methods. However, characterization costs time and money, and as such the minimization of effort in characterization is important for motor and drive system manufacturers. In order to evaluate the sensitivity of performance to characterization, two characterization procedures with different levels of measurement accuracy are performed in this section. The first is a detailed characterization which measures high frequency values of the machine quantities during operation. The second uses the quantities the inverter observes during operation. The simple sensitivity measure from section 2.2.3 is used to determine the sensitivity to characterization by measuring torque controller performance at two points, 800 and 1500 RPM 30, 40 and 50 $N \cdot m$. Note that in the analysis, no error is introduced in the parameters. The entire process from characterization to sensitivity calculation is performed in the search for the most accurate results. With this analysis, the time which must be spent on characterization can be minimized, by not characterizing the lowest sensitivity quantities accurately.

Another characterization was performed on a small test IPM machine. The machine being characterized is a 10kW Samarium Cobalt magnet interior permanent magnet machine. A setup is used – shown in Fig. 3.15 – to find the sensitivity for this IPM machine. This setup consists of a DC machine rated to operate at torques exceeding the IPM machine torque and speeds of 2650 RPM, above the base speed of the IPM machine being characterized. The DC machine is driven by a thyristor drive system. The DC machine acts as a generator while the IPM machine is driven as a motor during characterization. Using the same sensors as the SPM machine setup, a torque sensor, high frequency current, and voltage sensor is used to gather data for machine characterization. The IPM machine is driven by an APS inverter with the Texas Instruments floating point DSP TMS320F28335. The machine is given commands like the SPM machine setup. The inverter, CAN setup and CAN acquisition was done by Jorge Cintrón-Rivera. Data is gathered in two ways. The first way data is gathered is by the use of a high frequency $1.25\frac{GSamples}{Second}$ scope to record the data form the high frequency voltage and current sensors. The incremental encoder zeroing pulse, which signifies the completion of one mechanical rotation, is used to determine the relationship between the voltage, current, and the position of the machine rotor by acting as the trigger. This relationship between electrical quantities and rotor position is required for characterization in the two phase frame of reference. A second simplified method of characterization [2] is implemented to see how sensitive the final controller operation is to the machine characterization method. This uses data gathered from voltage, current and position sensors on the inverter and then transmitted through CAN to the Labview interface program, where they are recorded on a computer.

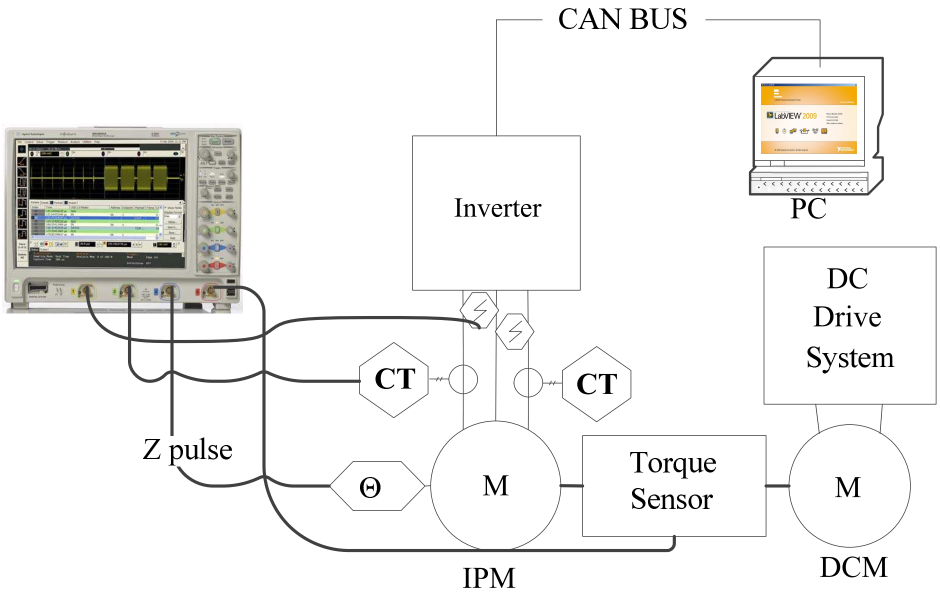

Figure 3.15: Physical test setup for IPM machine characterization with inverters, machines and sensors

3.4.1 Flux Linkages

The flux linkages were found from the methods discussed in sections 3.2.1. The flux linkages were found from the scope characterization method shown in Fig. 3.8 to be as in Figs. 3.16 and 3.17. These will then be used to calculate the controller.

Similarly the flux linkages were found from the simplified characterization setup shown in Fig. 3.15. The flux linkages are shown in Figs. 3.18 and 3.19.

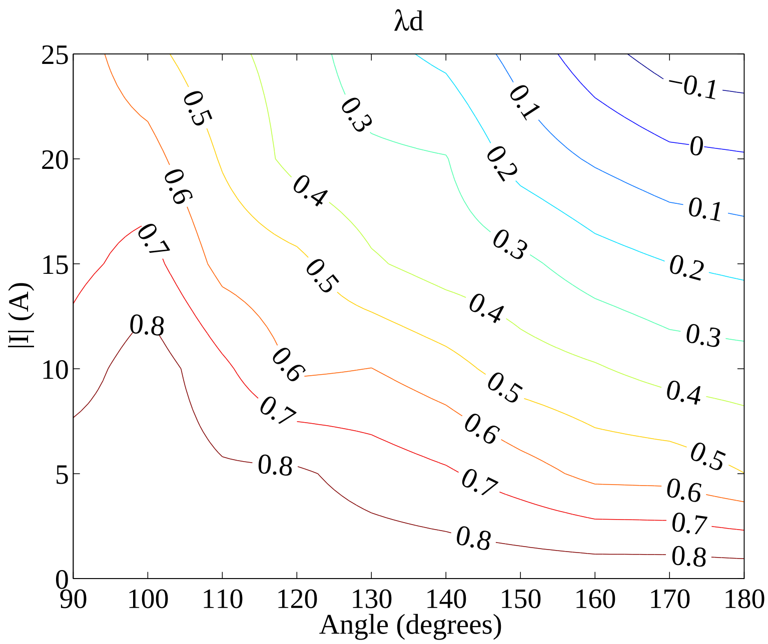

Figure 3.16: Current dependent direct axis flux linkage

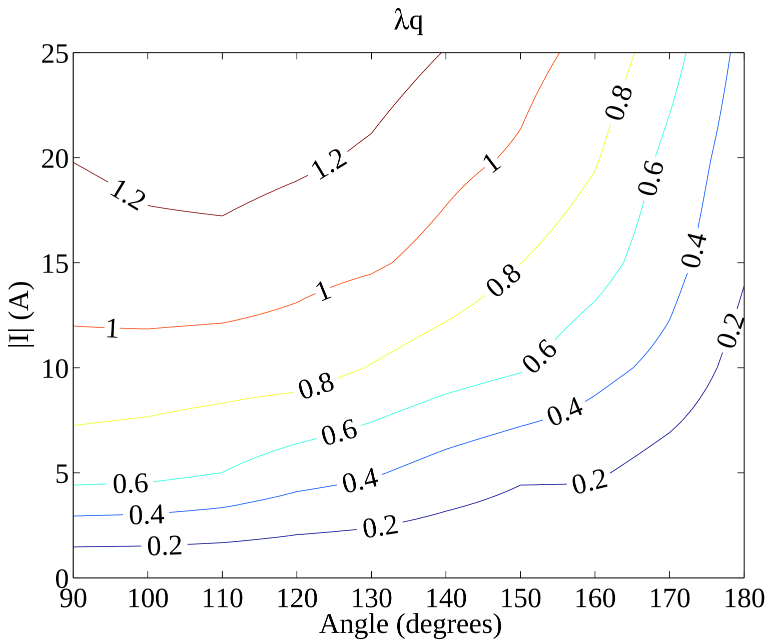

Figure 3.17: Current dependent quadrature axis flux linkage

3.4.2 Controller Development

The controller was extracted such that all operating points are within the maximum torque curve of the torque/speed in Fig. 3.20. With this information, the lookup tables are extracted

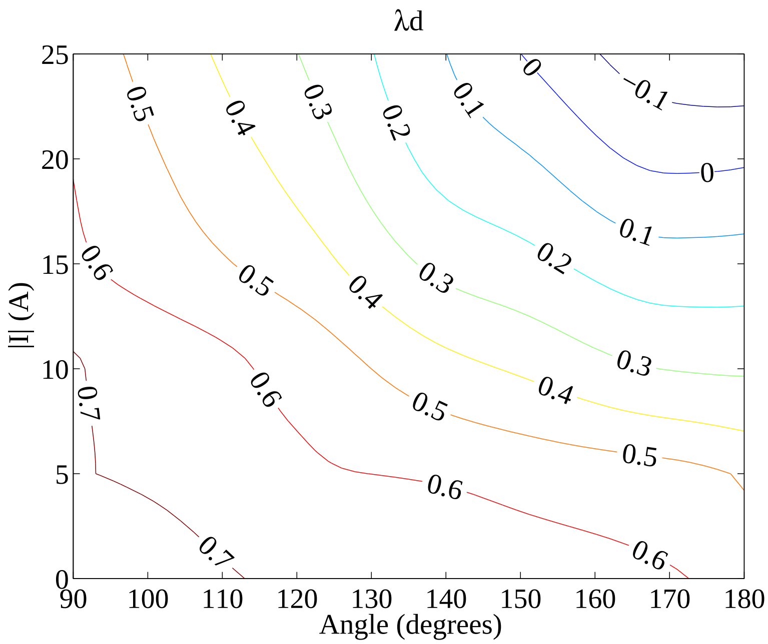

Figure 3.18: Direct axis flux linkage from simplified method from Jorge Cintrón-Rivera

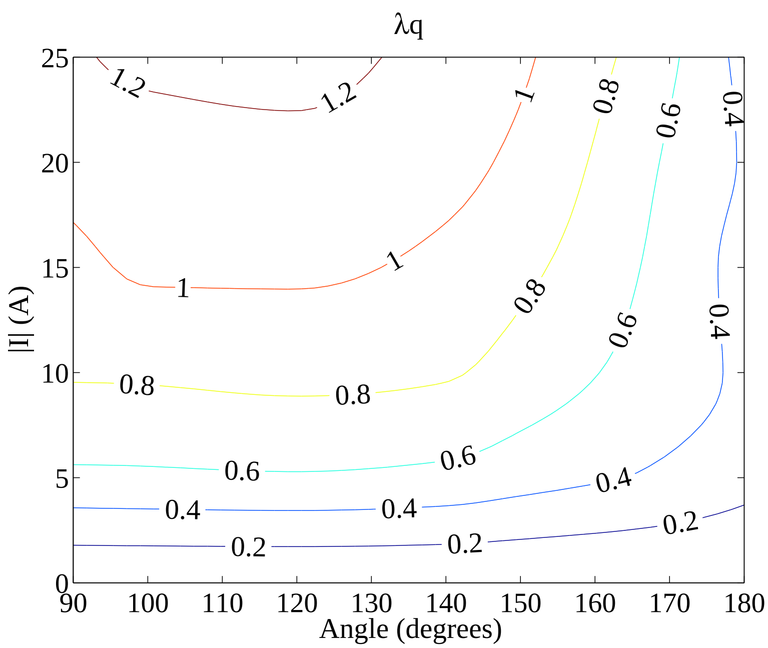

Figure 3.19: Quadrature axis flux linkage from simplified method from Jorge Cintrón-Rivera

for use in the controller. The interpolation step of controller development smooths the controller, the controller is given in Figs. 3.22 and 3.23. Similarly the fluxes from the simplified characterization are used to generate a controller in Figs. 3.24 and 3.25.

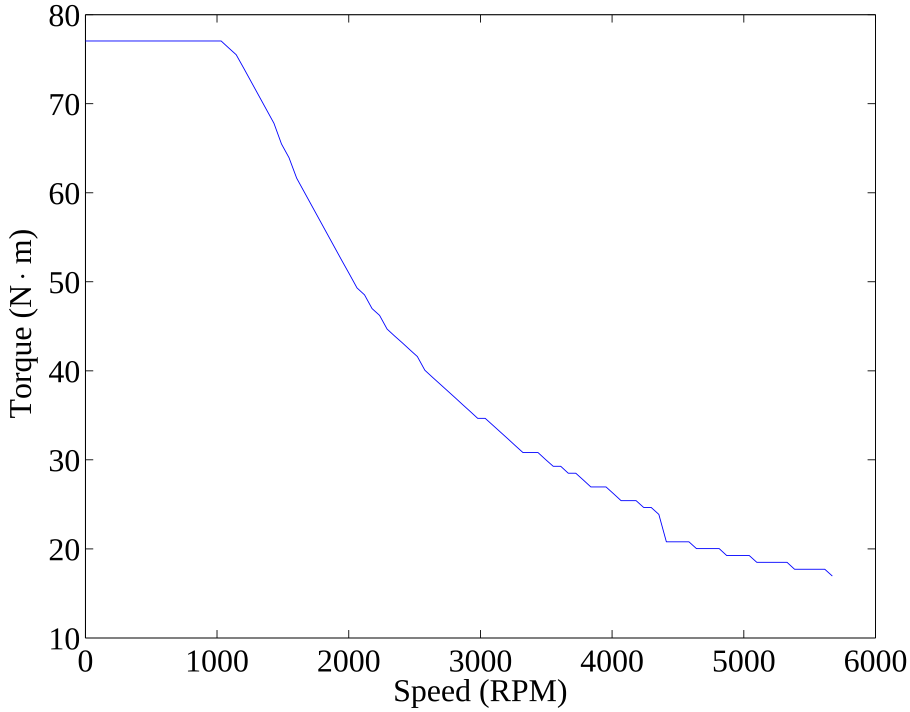

Figure 3.20: Torque-speed curve for the nominal controller

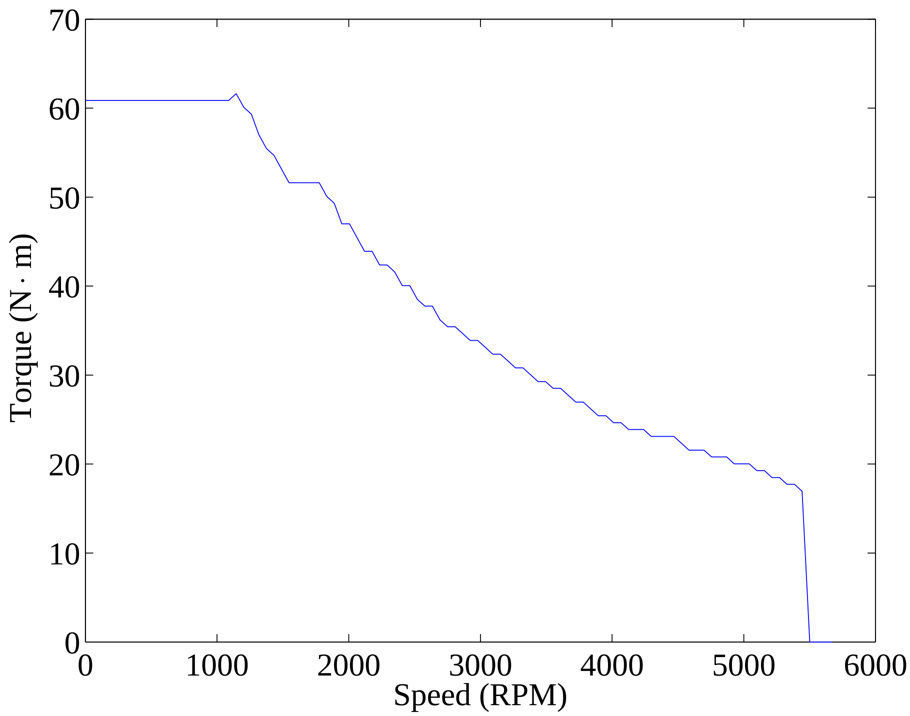

Figure 3.21: Torque-speed curve for simplified characterization flux linkage controller

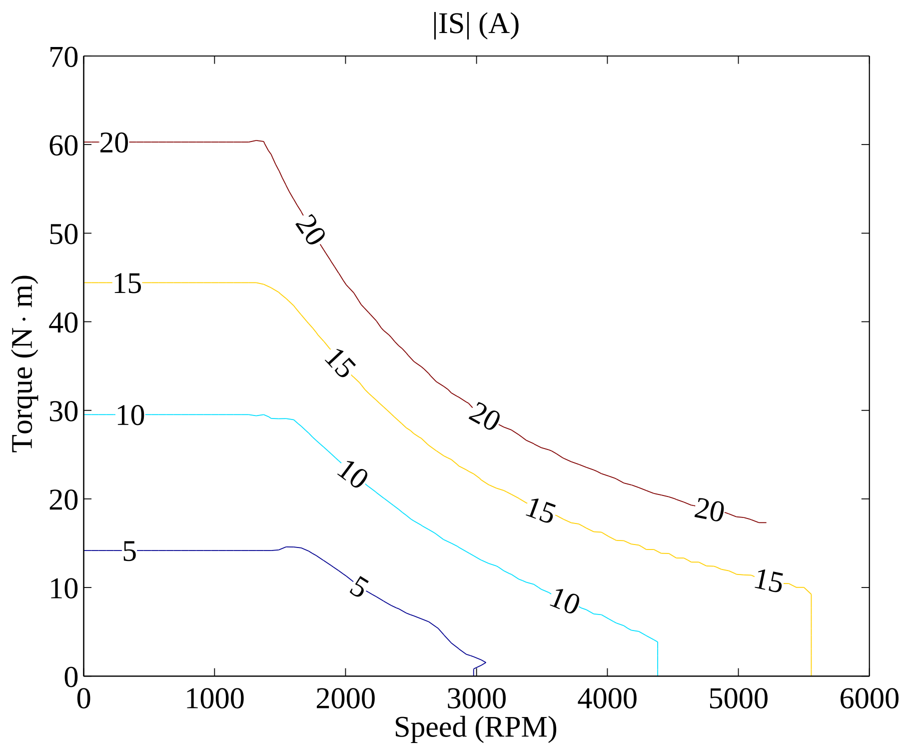

Figure 3.22: Operating point dependent current magnitude command

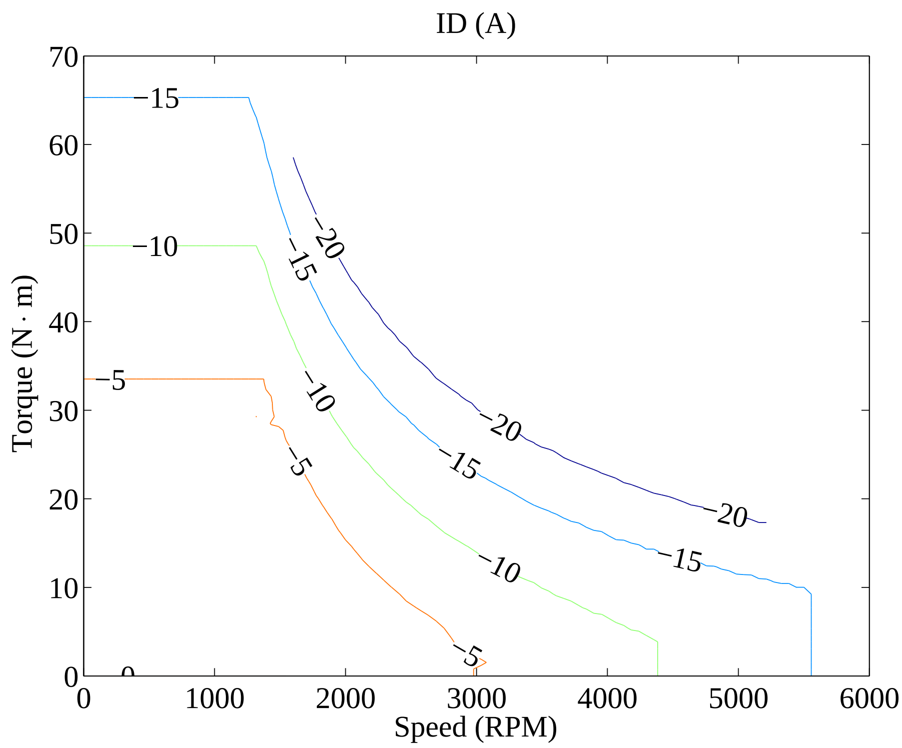

Figure 3.23: Operating point dependent direct axis current command

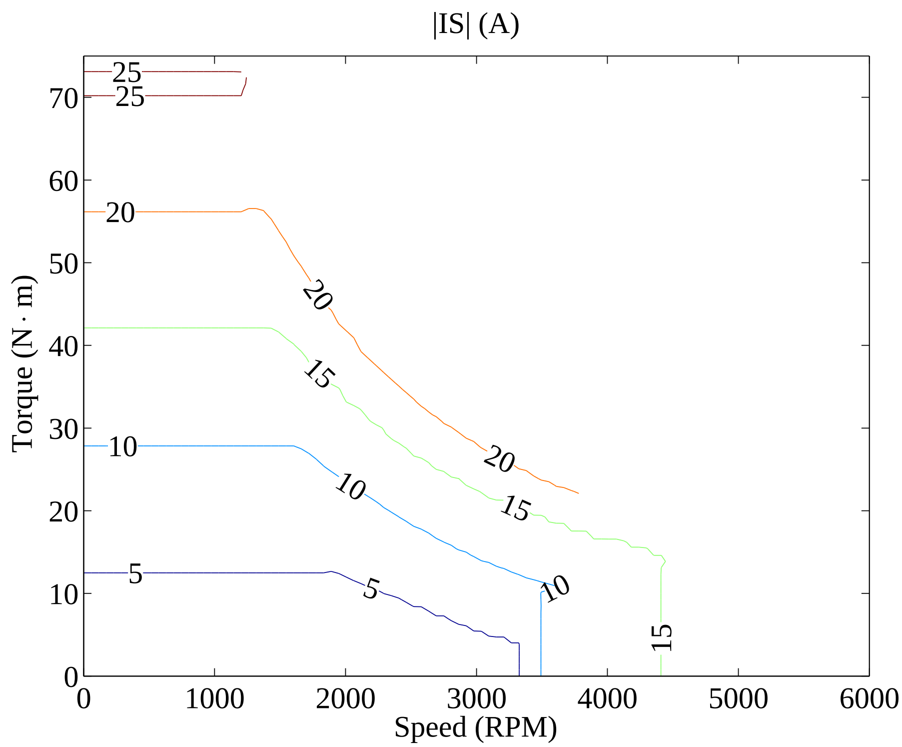

Figure 3.24: Operating point dependent current magnitude command from simplified characterization

3.4.3 Sensitivity Results

Once the controllers are extracted, various performance tests were completed with the machine test setup. The tests of interest here are intended to cover the range of operating points below and above base speed with a range of torques. The machine was operated at both 800 RPM and 1500 RPM speeds held constant while changing the torque command from 30 $N \cdot m$ to 40 $N \cdot m$ in the 800 RPM case and 30 $N \cdot m$ to 50 $N \cdot m$ in the 1500 RPM case. During these tests, the torque, voltage, current, speed and current commands are measured in real time. The torque was calculated based upon estimated flux and current to compensate for poor torque sensor accuracy. This was used to calculate the power and efficiency measures. These quantities are then used with the sensitivity measure from section 2.2.3 to calculate the sensitivity. The sensitivity was calculated with respect to the fluxes with the

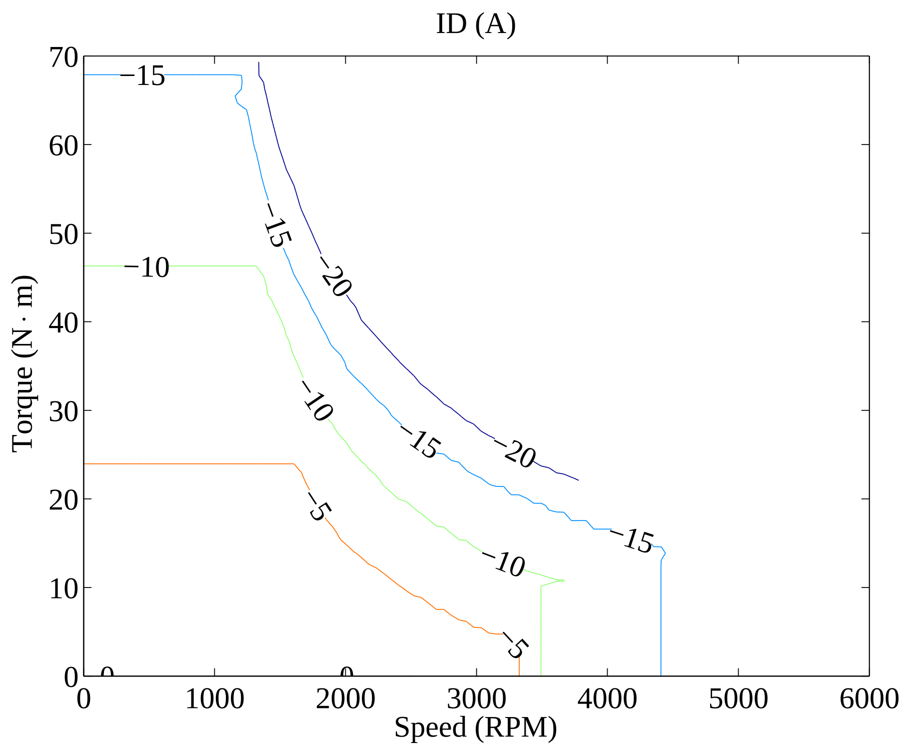

Figure 3.25: Operating point dependent direct axis current command from simplified characterization

results in Table (3.10).

While no error was artificially imposed in the system, small changes occur and this is what was measured. For this reason, the sensitivity measure for torque and power is high with respect to the quadrature axis flux. This is because the magnet torque is most affected by the quadrature axis flux. In most cases, the sensitivity of the output torque and power performance with respect to direct axis inductance is small due to the lesser dependence of these upon saliency torque. The efficiency sensitivity is very low. This is because the existence of flux error changes the performance through the current command at a certain torque and speed operating point. The new operating point will be different, but the losses for that point will be on the same magnitude in any case. The direct and quadrature axis currents greatly affect the machine controller. The large sensitivity of these quantities result from the dependence of the controller upon the flux linkages. The controller was derived from the maximum torque per ampere line, which coincides with the maximum operating voltage above base speed. If the fluxes are different, the voltage induced will also change. This means that the maximum voltage predicted changes. From this, the current command derived changes due to the change in voltage.

Table 3.10: Table showing the experimentally determined sensitivity to parametric error

-	$\Delta_{\xi \to P}$	T	P_m	P_e	η	I_d	I_q
800 (RPM)/30($N \cdot m$)	λ_d	0.034	0.036	0.067	0.1	2.492	0.375
-	λ_q	0.176	0.187	0.346	0.524	13.01	1.96
800 (RPM)/40($N \cdot m$)	λ_d	0.061	0.688	0.58	0.122	1.069	0.101
-	λ_q	0.269	0.602	0.507	0.107	0.9361	0.088
1500 (RPM)/30($N \cdot m$)	λ_d	0.061	0.061	0.052	0.112	0.382	0.253
-	λ_q	0.269	0.27	0.23	0.49	1.68	1.113
1500 (RPM)/50($N \cdot m$)	λ_d	0.622	0.62	0.583	0.048	0.448	0.107
-	λ_q	0.782	0.782	0.583	0.061	0.563	0.135

To make the relationship between the torque and errors in flux linkage clear, simulations were performed by applying both the simplified and detailed controllers from Figs. 3.22 and 3.23 as well as 3.24 and 3.25, respectively, to the detailed machine model given in Figs. 3.16 and 3.17. This results in two sets of torques and two sets of fluxes, from which the controllers are derived. These can be used with equation (2.56) to find the sensitivity over the entire operating range of the drive. From this, it is clear that the developed torque is sensitive to λ_d in the field weakening region, as the currents are determined in field weakening based upon the predicted λ_d. Further, note that the sensitivity of torque to λ_q is high in the high torque low speed region, as the torque estimate is not as reliant upon the field weakening calculation, and thus λ_d, but upon the magnet flux linkage, and thus λ_q.

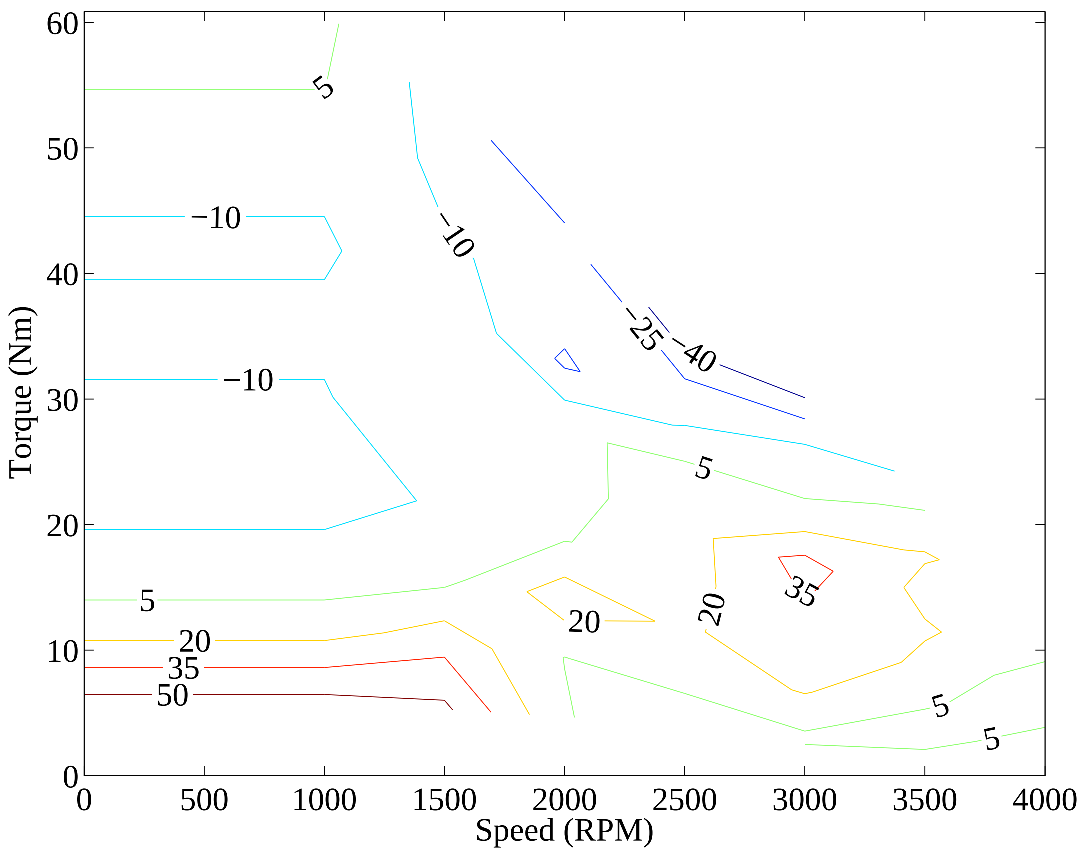

Figure 3.26: Direct axis torque sensitivity with respect to operating point ($\Delta_{\lambda d \to T}$)

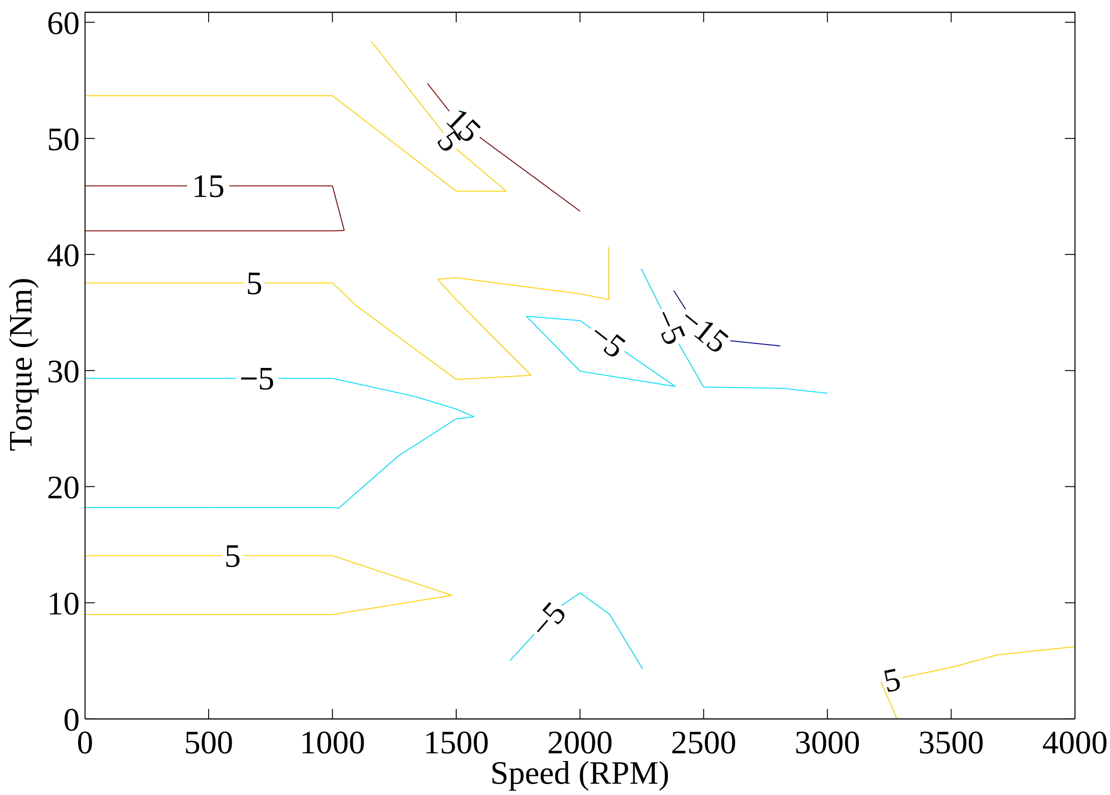

Figure 3.27: Quadrature axis torque sensitivity with respect to operating point ($\Delta_{\lambda q \rightarrow T}$)

Chapter 4

Conclusion

This thesis details the effect of error in parameters upon the output performance and sensitivity. Knowing the effect that errors in the parameters have upon the output performance can at least allow for more accurate determination of the most important parameters. A method was also reviewed from literature to accurately determine parameters, including the exact setups used. It then details a controller from literature, which measured performance with an experimental test, finite element simulation, and an analytical model simulation. The controller parameters then have error induced to observe the change in performance. This effect of error in each parameter is compared, using various metrics for three machines, to determine which parameter has the greatest effect upon control. Another test used this sensitivity measure to determine the sensitivity of machine performance to characterization. A sensitivity measurement is used to compare the output sensitivity to error in various parameters.

For the SPM machine, torque is found to be most affected by the quadrature axis inductances as well as flux linkage due to the magnets. Thus, for areas where torque accuracy is required, these parameters should be most accurately determined. The settling time is most affected by the inductances and flux linkage due to the magnets, so if a fast transient response is desired the inductances and flux linkage due to the magnets should be determined very closely to the actual value. Finally, the steady state error can be found to be most affected by the flux linkage due to the magnets, so where high current accuracy is required on the output, these quantities should be accurately found. As the current controller does not vary with the machine topology, the current sensitivity is generalized to any machine.

For the first IPM machine, the flux linkage due to the magnets was also seen to affect the torque and power performance. The resistance was not found to be of great importance where machine performance is concerned. The results differ from the salient machine in that the controller development is heavily dependent upon the axis inductances. This is because the saliency is vital in the development of torque. Thus, when designing controllers, the characterization should accurately determine the inductances. The change in these parameters were also seen to heavily affect the expected operating range of the machine.

The second IPM machine was used to determine the sensitivity of performance to the entire characterization process without any introduced errors. Characterization error was found by a process of characterizing the IPM machine with two different methods. Once more, the SPM machine and FEA from the first IPM machine results were verified. Even while characterizing with the best effort, the resultant parameters from the two characterization methods differed. The sensitivity of the controller to flux error was shown. It was seen that generally the quadrature flux axis has the largest effect on performance. This is not true for all operating points; some operating points have a greater sensitivity to the flux parameter error. The sensitivity of torque to λ_d is highest in the field weakening region. And further, the sensitivity of torque to λ_q is high in the high torque low speed region.

The importance of using accurate models, characterization methods, and accounting for faults is demonstrated by showing that when these are lacking, errors occur in performance. Torque error was clearly a result of changes in λ_d, especially in field weakening. This error can easily occur, as rotor eccentricity, heating of the magnets, and uniform demagnetization cause changes in the direct axis flux. Torque error also resulted from λ_q, especially where field weakening was not present, where magnet torque dominates. The quadrature axis flux is also important to know well, as saturation reduces the expected flux at high currents. Overall, errors in the flux, a direct result of poor modeling, poor characterization, or faults have a detrimental effect on performance.

In this thesis parameter dependent controllers are discussed. Parametric error causes the voltage applied for a given current command to be incorrect. Since the torque controller depends upon the parameters to determine the correct current operating point, the current operating point will be incorrect with parameter error. By developing a controller which estimates the parameters online, the controller can then be changed. In order to account for the change in parameters while maintaining robust operation, a controller implemented in tandem with the online parameter estimation would result in a controller not only robust to disturbance, but also to parametric error. A controller which can operate a PMSM or IPM machine through a combination of adaptive and robust control schemes and accomplishes a minimization of the sensitivity quantity would succeed in attaining a higher degree of performance.

These results guide the development of high performance controllers, as the output performance accuracy can be enhanced by accurate determination of the parameters which induce a larger performance error. To clarify, the flux linkage due to the magnets could be accurately known for all currents and temperatures if accurate magnetic torque performance is desired. By understanding this analysis, the results of applications requiring PMSMs and IPM machines can be improved. With more accurate controllers, smaller machines can be used since a "margin of error" is not required with increased efficiency; the machine does not need to be overdesigned. The controller response can also be improved as dependence on integral action is lessened, and thus are transient losses. This information can be used to guide the development of a controller and demonstrate whether a controller can effectively compensate for parametric error if sensitivity is reduced.

BIBLIOGRAPHY

BIBLIOGRAPHY

[1] Andrew S. Babel, Shanelle N. Foster, Jorge G. Cintron-Rivera, and Elias G. Strangas. Parametric sensitivity in the analysis and control of permanent magnet synchronous machines. In *Electrical Machines (ICEM), 2012 XXth International Conference on*, pages 1034–1040, 2012.

[2] Jorge G. Cintron-Rivera, Andrew S. Babel, Eduardo E. Montalvo-Ortiz, Shanelle N. Foster, and Elias G. Strangas. A simplified characterization method including saturation effects for permanent magnet machines. In *Electrical Machines (ICEM), 2012 XXth International Conference on*, pages 837–843, 2012.

[3] Jongman Hong, Sanguk Park, Doosoo Hyun, Tae june Kang, Sang Bin Lee, C. Kral, and A. Haumer. Detection and classification of rotor demagnetization and eccentricity faults for pm synchronous motors. *Industry Applications, IEEE Transactions on*, 48(3):923–932, 2012.

[4] M. Kazerooni and N.C. Kar. Methods for determining the parameters and characteristics of pmsm. In *Electric Machines & Drives Conference (IEMDC), 2011 IEEE International*, pages 955–960. IEEE, 2011.

[5] Ramu Krishnan. *Permanent Magnet Synchronous and Brushless DC Motors*. CRC Press, 2010.

[6] W. Leonhard. *Control of Electrical Drives*. Springer, 2001.

[7] K. M. Rahman and S. Hiti. Identification of machine parameters of a synchronous motor. *IEEE Transactions on Industrial Applications*, 41:557–565, 2005.

[8] Quntao An Li Sun. On-line parameter identification for vector controlled pmsm drives using adaptive algorithm. In *IEEE Vehicle Power and Propulsion Conference (VPPC), September 3-5, 2008, Harbin, China*, 2008.

[9] Paul Waide and Conrad U. Brunner. Energy-efficiency policy opportunities for electric motor-driven systems. Technical report, International Energy Agency, 2011.

[10] S.D. Wilson, P. Stewart, and B.P. Taylor. Methods of resistance estimation in permanent magnet synchronous motors for real-time thermal management. *Energy Conversion, IEEE Transactions on*, 25(3):698–707, 2010.

[11] Muhammad Jawad Zaheer. Tool for quality testing of raw material of permanent magnets. Master's thesis, Michigan State University, 2012.

[12] M. F. Hu W. Y. Lim K. W. Zhong, L. Rahman. Analysis of direct torque control in permanent magnet synchronous motor drives. *IEEE Transactions on Power Electronics*, 12:528–536, 1997.